THE CORTICAL EFFECTS OF OBJECT AFFORDANCES ON MOTOR ACTION
PRIMING USED IN RAPID BALANCE RECOVERY ACTIONS

THE CORTICAL EFFECTS OF OBJECT AFFORDANCES ON MOTOR ACTION
PRIMING USED IN RAPID BALANCE RECOVERY ACTIONS

By STEVIE FOGLIA, B.Sc.

A Thesis Submitted to the School of Graduate Studies in Partial Fulfilment of the
Requirements for the Degree Master of Science

McMaster University MASTER OF SCIENCE (2019) Hamilton, Ontario (Kinesiology)

TITLE: The Cortical Effects of Object Affordances on Motor Action Priming Used in

Rapid Balance Recovery Actions AUTHOR: Stevie Foglia, B.Sc. (McMaster University)

SUPERVISOR: Professor J.L. Lyons NUMBER OF PAGES: xi, 103

ABSTRACT

There is considerable evidence to suggest that object affordances (see Gibson, 1966) can serve to moderate volitional responses by "priming" the visuomotor system toward certain actions (e.g., Tucker & Ellis, 1998). Typically, these studies assume that shorter voluntary reaction time latencies reflect more efficient movement planning. Questions remain however, as to whether object affordances offer the same motor priming benefits in situations where the temporal window to initiate motor action precludes volitional movements (e.g., during an unexpected balance perturbation). The efficiency of balance reactions to a perturbation is dependent upon the ability for the motor system to generate short latency actions at the onset of instability. Due to the rapid nature of these actions, they are suggested to be regulated by information received prior to the perturbation. In this study, participants sat in a custom-built chair that delivered posterior perturbations and, on each trial, were presented with two of three types of stimuli within their reach (two graspable poles that varied in orientation and a flat non-graspable control). They were instructed to reach and grasp one of the poles at the moment of perturbation so as to mitigate the tilt. To assess cortical activity that may be indicative of motor planning in response to the perception of object affordances, changes in oxyhemoglobin (oxy-Hb) in the right and left premotor cortices were measured using a continuous wave fNIRS system. Results revealed a significant increase ($F= 4.62$, $p= .043$) in oxy-Hb in the right and left hemisphere (M = .023 µM) in response to objects that afford an optimal form of grasping action (mitigating excessive supination or pronation of the hand), compared to when no grasping opportunity was present (M = -.051 µM). These results suggest that affordances may be used to prime the system in the event of a balance threat.

ACKNOWLEDGEMENTS

I would like to express my deep gratitude to my thesis supervisor Dr. Jim Lyons, Professor, Department of Kinesiology at McMaster University for his guidance throughout the planning and development of this research work. His constructive suggestions and mentorship have been invaluable throughout this research process. I would also like to thank my supervisory committee, Dr. Mike Carter, Assistant Professor, Department of Kinesiology at McMaster University, Dr. Peter Keir, Professor, Department of Kinesiology at McMaster University and Dr. Luc Tremblay, Associate Professor, Faculty of Kinesiology & Physical Education, University of Toronto, for their valuable inputs and support throughout this research process.

I would also like to thank my parents Anna and Steve for all their love and encouragement throughout my study.

TABLE OF CONTENTS

4.0 RESULTS

5.0 DISCUSSION

6.0 REFERENCES

LIST OF FIGURES AND TABLES

LIST OF ALL ABBREVIATIONS

AIP- Anterior intraparietal area

ATP- Adenosine triphosphate

BA6- Brodmann area 6

C C- Control object (light side) and control object (right side)

C LR- Control object (light side) and left to right orthogonal (right side)

C RL- Control object (light side) and right to left orthogonal (right side)

C- Control object

CSF- Cerebral spinal fluid

CSP- Cerebral spinal fluid

cTBS- Continuous theta burst transcranial magnetic stimulation

d-d- Dorso-dorsal stream

Deoxy-Hb- Deoxygenated hemoglobin

F2- Dorsal premotor cortex

F4- Premotor ventral caudal area

F5- Premotor cortex

F6- Pre-supplementary motor cortex

fMRI- Functional magnetic resonance imaging

fNIRS- Functional near-infrared spectroscopy

GMD- Grey matter detection

HRF- Hemodynamic response function

ICMS- Intracortical microstimulation

LED- Light emitting diode

LR C- Left to right orthogonal (left side) and control object (right side)

LR LR- Left to right orthogonal (left side) and left to right orthogonal (right side)

LR Orthogonal- Left to right orthogonal

LR RL- Left to right orthogonal (left side) and right to left orthogonal

M1- Primary motor cortex

MA- Motion artifact

MEP- Motor evoked potential

MNI- Montreal Neurological Institute

MRI- Magnetic resonance imaging

Oxy-Hb- Oxygenated hemoglobin

PCA- Principal component analysis

PMd- Dorsal premotor cortex

PMv- Ventral premotor area

PPA- Physical property affordance

Pre-SMA- Pre-supplementary motor area

RL C- Right to left orthogonal (light side) and control object (right side)

RL LR- Right to left orthogonal (light side) and left to right orthogonal (right side)

RL Orthogonal- Right to left orthogonal

RL RL- Right to left orthogonal (light side) and right to left orthogonal (right side)

RT- Reaction time

S1- Primary somatosensory cortex

SCD- Scalp to cortex distance

SMA- Supplementary motor area

TMS- Transcranial magnetic stimulation

tPCA- Target principal component analysis

v-d- Ventro-dorsal stream

DECLARATION OF ACADEMIC ACHIEVEMENT

I, Stevie Foglia, declare this thesis to be my own work. I am the sole author of this document. No part of this work has been published or submitted for publication or for a higher degree at another institution. To the best of my knowledge, the content of this document does not infringe on anyone's copyright. My supervisor, Dr. Jim Lyons, and the members of my supervisory committee, Dr. Luc Tremblay and Dr. Peter Keir and Dr. Mike Carter have provided guidance and support at all stages of this project. I completed all of the research work.

1.0 LITERATURE REVIEW

1.1 Ecological Psychology and its Application in Motor Control

According to the ecological perspective of motor control, the environment can be viewed as a collection of natural factors with the potential to exert influence on the perceiver through action possibilities associated with objects within that environment. The information from these objects is perceived by the human system continuously and directly such that any act, which may be completed with an object, is driven by the meaning perceived from the organism interacting within that environment (Marteniuk, 1976; Posner, 1982). Central to this ecological perspective is the concept of affordances. As described by Gibson (1979), affordances define objects in such a way that they are not only a fact of the environment, but also a fact of behavior. It is therefore, the sensorimotor capabilities of the perceiver that constrains the kind of information that is accessed regarding an object of interest and the meanings associated with it. These are taken as any actions that are "afforded" to the system by that object (Michaels & Carello, 1981). Using a stimulus response voluntary reaction time paradigm, Tucker and Ellis (1998) demonstrated that affordances facilitate movement by decreasing reaction time (RT) when the response effector was aligned spatially with the object such that it would afford an action. (e.g., the handle of a mug was ipsilateral to the hand of response). Left-right coding was proposed to account for this compatibility effect as based on the organization of the visuomotor system. The authors concluded that certain action-related information, in this case the hand most suited to grasp the object, is represented automatically when the object is viewed in peripersonal space (i.e., participants are better able to identify salient object

characteristics when object affordances are aligned in such a way to be compatible with action) (Tucker & Ellis, 1998). Specifically, the object better affords the action of grasping when the graspable area is oriented toward the hand predisposed for action. This effect of object orientation on response latency is consistent with an affordance account based on automatic activation.

Physical property affordances (PPA's) is the term currently used to describe these characteristics of objects that are suggested to prime motor interactions with that object by encompassing action relevant features and orientations within their physical makeup (Symes, Ellis & Tucker, 2006). Previous work, also using stimulus-response RT paradigms, has shown that choice RT is facilitated when response effectors are aligned spatially with the presented PPA, and that these extend to reflect the response effectors alignment with the object orientation (Foglia & Lyons, 2018). For example, when the orientation of an object is aligned with a response hand in such a way that a grasp would be anatomically optimal (i.e., minimizing excessive pronation and supination of the hand) responses to objects expressing those PPAs were facilitated. As such, behavioral outcomes are suggested to be modulated as a function of object orientation, where priming benefits are mediated by varying orientations of the same object. This facilitation may result as a function of the sensorimotor priming of a volitional response occasioned by specific PPAs.

Object grasping is a ubiquitous, highly-specialized behavior that presents challenges to the human motor system, mainly as a result of the coordination of specific grasping configurations of the hand (Jeannerod et al., 1995, Macfarlane & Graziano, 2009). To account for this, the object representation and potential motor acts of object physical

features are cortically interconnected (Rozzi & Coudé, 2015). As a result, a complex organization of cortical regions are involved in perception and action execution towards objects that can be interacted with, or in essence all objects in one's peripersonal space.

1.2 Neurophysiological Representation of Physical Property Affordances

Two forms of parallel processing occur in response to a presented object: a semantic description that is generated by higher order cortical visual areas and a pragmatic description that involves the processing of PPA's and their translation into their action possibilities, or affordances (Ellis & Tucker, 2000). Specifically, this processing has been suggested to occur through two visual streams: termed ventral and dorsal (Goodale & Milner, 1992; 1982). The ventral (occipito-temporal) stream links the primary visual cortex to the inferotemporal regions and is sensitive to information regarding object identity, that thereby enables construction of a cortical representation of what is in the environment. The dorsal (occipito-parietal) stream, which terminates in the parietal region, contains neurons sensitive to spatial information that mediate visually-guided actions (Ungerleider & Mishkin, 1982). Ultimately, the dorsal stream builds a cortical representation of where things are in the environment. The dorsal stream can be further subdivided into the dorso-dorsal (d-d) and the ventro-dorsal (v-d) streams (Rizzolatti & Matelli, 2003). While the d-d stream maintains commonality with the function of the dorsal stream, the v-d stream is involved in the sensorimotor transformation of visual information for grasping, the perception of space and the recognition of action.

Within the v-d stream, the anterior intraparietal area (AIP) and ventral premotor area (PMv), are of particular importance in the application of object grasping, specifically

the transformation of object properties into the corresponding possibility for grasping actions (Rizzolatti & Matelli, 2003). AIP neurons are responsible for encoding the geometrical features shared by different objects and can be divided functionally into three classes: motor-dominant, visual and motor, and visual-dominant (Taira et al., 1990; Sakata et al., 1995; Murata et al., 2000). PMv is responsible for encoding motor acts performed with the hand or mouth (Kurata & Tanji, 1986; Gentilucci et al., 1988; Rizzolatti et al., 1988; Hepp-Reymond et al., 1994; Ferrari et al., 2003). Specifically, a large portion of these neurons are responsible for encoding specific motor acts such as grasping, with unique activation based on the specific type of grip to be used, such as precision, finger prehension or whole hand prehension (Rizzolatti et al., 1988).

The AIP region has monosynaptic connections with several brain regions such as PMv (Luppino et al., 1999; Borra et al., 2008, Gerbella et al., 2011). Contained within the PMv region are neurons that have been shown to discharge to the visual presentation of graspable objects, with activity being mediated by the actual characteristics of the perceived object. A specific selectivity is seen based on the size and shape of the presented object (Murata et al., 1997; Raos et al., 2006). These are known as canonical neurons (Rizzolatti & Fadiga, 1998). It has been suggested that the presentation of objects produces a physical property dependent representation of the observed object in terms of a potential grasping action towards that object. This process occurs irrespective of whether or not there is an actual intention to act on these objects. Magnetic stimulation (rTMS), has been used to demonstrate that PMv-primary motor cortex (M1) interactions during a grasping movement are reliant on object properties being perceived and integrated by AIP (Davare, Rothwell

& Lemon, 2010). The integration of object properties occurs sequentially from AIP-PMv-MI along a gradient axis (Murata et al., 1997; Murata et al., 2000; Raos et al., 2006). Thus, the AIP region is of particular importance, as disruption will interfere with activity of downstream regions (Davare, Rothwell & Lemon, 2010). Furthermore, temporary inactivation of AIP or the PMv region results in interference with grasping performance (Fogassi et al., 2001; Gallese et al., 1994; Davare et al., 2007; Davare et al., 2006; Rice, Tunik & Grafton, 2006). Therefore, AIP plays a critical role in integrating sensory information required for grasping.

When the system is at rest, canonical neurons in PMv and object-related neurons in AIP have low firing rates. However, when an object that can be grasped is presented, populations of neurons within AIP responsible for providing information regarding object properties, such as size and shape, increase their firing rate (Murata et al., 2000; Raos et al., 2006). This information is suggested to be transferred to specific populations of neurons within PMv. Subsequently, due to the facilitating drive of information from AIP, canonical neurons in PMv also begin to increase their firing rate and provide outputs to M1 (Davare, Rothwell & Lemon, 2010). As a result, it has been suggested that inputs from AIP neurons is required in order to modulate the excitability of PMv and M1. This excitability, however, is context dependent as well as grasp specific as disruption to AIP at rest had no effects on PMv or M1 excitability. It was only when graspable stimuli were presented to the system that these modulating pathways from AIP were impactful on PMv and M1 excitability (Davare, Rothwell & Lemon, 2010). It has been suggested that the deficits observed in AIP and PMv during virtual lesion induction are a result of a reduction in the quantity of visual

information regarding object properties that are transferred to PMv, ultimately reducing the ability to generate specific motor plans aimed at those objects (Davare, Rothwell & Lemon, 2010). This line of thinking suggests that the object properties integrated in AIP form an object reference frame that is transferred to PMv to create a grasp reference frame. The manner in which object property information from AIP is integrated in the formation of motor plans is, however, still unknown. One possibility is that intrinsic characteristics of the object (e.g., its size, shape and orientation) are matched with a motor plan for the specific grasp that would be most optimal for interacting with them (Davare, Rothwell & Lemon, 2010). Thus, it is reasonable to suggest that the physiological basis for Gibson's Affordance Theory lies within the AIP-PMv-M1 axis.

The primary motor cortex (M1) contains neurons that are reciprocally interconnected with parieto-frontal and premotor regions positioned on the dorsolateral and dorsomedial portions of the hemisphere (Rizzolatti & Luppino 2001; Grafton 2010; Davare et al. 2011; Fattori et al. 2015; Kaas & Stepniewska 2016; Maranesi et al. 2014). The AIP area, posterior parietal area (V6A), ventral premotor area (F5) and the ventro-rostral portion of the dorsal premotor cortex (PMd) contain visuomotor neurons that discharge during the presentation of graspable objects and during the execution of reach to grasp actions (Sakata et al. 1995; Baumann et al. 2009; Fattori et al. 2010; Fattori et al. 2012; Murata et al. 1997; Raos et al. 2006; Fluet et al. 2010; Bonini et al. 2014a; Vargas-Irwin et al. 2015; Raos et al. 2004). These networks exhibit a visual to motor response pattern that reflects the visuomotor transformation of object physical properties into the respective motor acts that are afforded by the object (Murata et al. 1997; Raos et al. 2006; Fluet et al. 2010; Bonini et

al. 2014a; Vargas-Irwin et al. 2015). This has especially been observed in area F5 (premotor cortex; Lanzilotto et al., 2016).

Area F6 (pre-supplementary motor cortex) is primarily responsible for selecting, triggering, or inhibiting actions (Matelli et al. 1991). This area functions to bridge prefrontal regions with dorsolateral premotor areas, specifically dorsal premotor cortex (F2), premotor ventral caudal area (F4) and F5. These areas are of particular importance in the control of actions involving the forelimb (Rizzolatti & Luppino 2001). Intracortical microstimulation (ICMS) studies in monkeys have reported the importance of F5 in regard to the control of multi joint forelimb movements (Luppino et al., 1991), while area F6 is of particular importance in preparing reach to grasp arm movements.

1.3 Affordance Motor Action Priming

Neurophysiological evidence from transcranial magnetic stimulation (TMS) studies show that cortical region activation, as evident through motor evoked potential increases, may be responsible for mediating affordance motor action priming. It has been illustrated that when an object affording a pinch or whole hand grasp is within the peripersonal space of the system, motor evoked potential (MEP) amplitudes are greater in muscles that would be utilized to take advantage of that grasp, even in the absence of any intention to act (Cardellicchio et al., 2011). Additionally, these MEP amplitude increases have been shown to wash out when an object that was previously presenting a handle for grasping is presented with the handle broken (Buccino et al., 2009). The action-perception system is specific enough in its integration of object visual features, that motor plans are represented prior to the commencement of action, in order to facilitate movement. This priming effect

has been demonstrated at latencies of 120, 200, 300 and 450 ms post-TMS stimulation to the primary motor cortex (M1) (Cardellicchio et al., 2011, Buccino et al., 2009; Makris & Stergios, 2011; Proverbio et al., 2011; Franca et al., 2012). This evidence suggests that the objects are not only perceived almost instantaneously by the system, but also have been integrated in terms of the object visual features that drive the motor plans that would be best suited to act. It can therefore be suggested that due to the rapid temporal sequence of these events, that a direct link between action and perception may exist (Tillas et al., 2017).

1.4 Perturbation Evoked Rapid Compensatory Actions

Balance reactions in response to a perturbation stimulus are characterized by changes in support to take advantage of either a lower body stepping reaction or upper limb prehension (Maki & Whitelaw 1993; Shumway-Cook & Woolacott, 1995; Maki & McIlroy, 1997; Jensen et al., 2001). As a result, the efficiency of these responses is dependent upon the ability of the system to generate short latency actions at the onset of instability. The onset of these actions has been illustrated to occur ~100 ms earlier than the same action performed voluntarily (Gage et al., 2007). As a result, postural responses to balance perturbations are a unique set of behaviors as they are reliably demonstrated to occur at a latency shorter than a voluntary movement, but longer than a spinal reflex (Chan et al., 1979; Diener et al., 1984; Ackermann et al., 1991; Jacobs et al., 2008).

Despite the temporal difference, parallel findings between perturbation and voluntary reach to grasp actions in both electromyography and kinematic data, suggest that a similar cortical mechanism is responsible for the control of both these movements (Gage et al., 2007). Specifically, the perturbation evoked movement response maintains the same

sequence of muscle activity and spatial-temporal characteristics as the voluntary reaching pattern. The current suggestion is that the system utilizes environmental information perceived prior to the fall to generate these actions (Gage et al., 2007).

Bolton et al., (2011) illustrated that cortical centers mediate perturbation-evoked reactions, specifically in terms of generating preparatory responses to unintended action possibilities. This has been suggested to be accomplished through anticipatory control that involves processes such as expectation, intention, and anxiety (Horak et al., 1989; Ackermann et al., 1991; Maki & Whitelaw, 1993; Gottlieb & Agarwal, 1980; McIlroy & Maki, 1993; Burleigh & Horak, 1996; Grin et al., 2007; Jacobs & Horak, 2007). These processes are considered in relation to the environment the system is facing, such as one that may be threatening to balance, such as walking on an icy surface. These processes ultimately affect the 'central set', which is a state of readiness of the system for a stimulus or movement (Jacobs, et al., 2008).

Scott's (2016) model of automatic control outlines the respective latencies of object perception that is triggered by sensory stimuli in response to perturbations to the system. For example, during the initiation of a fall, the vestibular system would detect changes in balance and spatial orientation that would allow the system to recognize it is in a state of threat. At an initial latency of 25 ms (R1) the first feedback response is generated (Rossignol et al., 2006; Zehr et al., 2004). This response does not display features that are related to goal-directed actions; however, it has an impact on higher level control systems through its ability to stop an ongoing corrective process (Kurtzer, et al., 2010). Following the R1 spinal-generated response, the R2 response occurs at 60 ms post perturbation (Scott

et al., 2015; Pruszynski & Scott, 2012; Kurtzer, 2014). This response is representative of the physics of the limb and also the environment that system currently occupies, including information regarding graspable objects (Kimura et al., 2006; Krutky et al., 2013; Kurtzer et al., 2009: Kurtzer et al., 2008; Shemmell et al., 2009; Soechting & Lacquaniti, 1988; Walker & Perreault, 2015; Crevecoeur et al., 2016). These findings are suggestive that the system is using information perceived prior to perturbation onset to drive these rapid R2 responses.

1.5 An Internal Model Posited Through Ecological Psychology

Two temporally separated events are considered by the system in relation to a balance perturbation (Mochizuki et al., 2010). First, the context in which the instability occurs. This includes information regarding the current state of the system (i.e., walking or standing), the environment it is facing (i.e., dry surface or wet surface) and objects contained within that environment. This information is used to build a visual spatial map that is continuously updated through visual inputs. This map is critical in allowing the system to recognize the environment and provide information regarding the possible nature of a perturbation should one occur (Jacobs & Horak, 2007; Gage et al., 2007). This information is used to ensure that the initial limb trajectory and transport phase of a compensatory reach to grasp action can be directed towards a target as quickly as possible (Maki & McIlroy, 1997; Ghafouri et al., 2004). Second, is the outcome of the perturbation, related to the magnitude, direction and velocity of the instability. This information is only received once the perturbation has been initiated. For example, wrist trajectory has been shown to be influenced by the direction of the perturbation, suggesting target specific

control responses initiated within 100 ms post perturbation (Gage et al., 2007). Planned actions are additionally crucial for generating a rapid stabilizing force once the support surface has been contacted (Gage et al., 2007). Perpetrator electromyography activity has been observed in the forearm, deltoid and triceps prior to hand contact. The upper limb is rapidly guided to the target until just prior to contact, where it is slowed down in order to allow for a greater probability of grasping and mitigating damage to the hand. As such, specific muscular control of limb geometry is occurring even at these short latencies (Gage, et al., 2007).

Once a loss of balance occurs, the spatial map is integrated with online multisensory information (e.g., magnitude, direction and velocity of the perturbation). The combination of these two streams of information produce a functional strategy that drives rapid targeted actions at regaining balance (Zettel et al., 2005; 2007; Cheng et al., 2012). This theory is supported through visual occlusion studies that report visual occlusion at the moment of perturbation onset does not impede the participant's ability to make target specific corrective actions, despite the characteristics of the perturbation being unknown prior to the fall (Ghafouri et al., 2004; Akram et al., 2013). Studies employing lower body stepping reactions to a whole-body perturbation have demonstrated that in the absence of online visual feedback, compensatory stepping actions are successful in an obstacle ridden environment (Zettel et al., 2007). It was reported that once perturbed, visual gaze was never redirected at any obstacles, or landing site, but was rather fixed substantially anterior to the step landing site. The information that drove these corrective actions was suggested to be perceived prior to perturbation onset (Zettel et al., 2005; 2007).

These results are consistent with an ecological model of internal environment representation. Specifically, it is the ability of an intact human motor system to continuously perceive sensory information from the environment that is collected to build an internal descriptive representation of objects in the external world (Marr, 1982). This internal representation does not require conscious attentional resources to generate and is thus free of impacting daily executive functioning (Cardellicchio et al., 2011). Additionally, this representation includes potential actions that the environment currently affords (Gibson, 1979; Fadiga et al., 2000; Cisek, 2001). These action potentials are updated to reflect the environmental parameters that are currently being faced by the system (Kalaska et al., 1998; Kim & Shadlen, 1999; Cisek, 2001; Gold & Shadlen, 2001; Cisek & Kalaska, 2005). This process takes into consideration object visual features in the environment present in both foveal and peripheral visual fields at a latency of 120 ms post object presentation (Akram et al., 2013; McDannald, 2018). As a result, the system's awareness of the environment occurs in a time frame that would be too long to recover from a balance perturbation if this process occurred directly at the onset of the fall.

As such, this begins to raise the question as to whether object visual features (PPA's), present in the optic array, are integrated by the system into this internal representation of the external world. It has been suggested that the same cortical networks involved in voluntary reach to grasp actions regulate perturbation evoked actions (Gage, et al., 2007, Bolton, et al., 2011). It is reasonable, based on this earlier evidence, to assume that the information regarding objects PPA's integrated by the AIP-PMv-M1 chain and other cortical networks would be used to generate preparatory strategies in premotor

cortical areas such as F5 and F6, in the event of an unintended balance perturbation. It is this assumption that leads directly to the research questions posed in this thesis: 1) To what degree does this preparation reflect the ability for the objects to be utilized by the system in situations of postural threat? 2) Is preparatory information modulated by the optimality of the object to afford a compensatory grasping action? 3) Is visual information perceived at the moment of perturbation onset sufficient to drive successful compensatory reach to grasp actions?

It is hypothesized that affordance information regarding objects in the peripersonal space and presumably integrated by the AIP-PMv-M1 chain is mediated by the potential for objects to be utilized in perturbed balance recovery actions. This will be reflected in the magnitude of concentration increases of oxygenated hemoglobin in the premotor cortices. Specifically, this increase would occur in the hemisphere representative of the limb that would be best suited to take advantage of that affordance, prior to perturbation onset. Thus, objects that would be most optimal (defined as the potential for an object to be used without excessive pronation or supination of the wrist) would produce the greatest concentration change increase.

1.6 Purpose

The objective of this study is to extend current research exploring the action-perception properties of affordances beyond volitional movements through studying innate mechanisms that drive and regulate balance in the event of unintended perturbations. The degree to which PPA's may be incorporated into a continuous environmental awareness that can then be used for both intended and unintended (i.e., during grasp-related actions to

reestablish balance) actions remains unclear. Specifically, this research addresses the question of whether/how PPA's are perceived and integrated by the system prior to a fall and to what degree this integration reflects the optimality of the object to be utilized in a potential situation of balance threat. This study, to the best of our knowledge, would be the first to test the influence that objects within the environment have on the priming of the perceptual-motor system in response to situations of threat, using hemodynamic measures of cortical activation. In this case, priming refers to the presentation of PPA's where activation of cortical regions responsible for planning reach to grasp actions occur as a direct result of the objects ability to afford compensatory action. By investigating the neurophysiological contributions relative to varying object affordances, this study linked ecological theory to neurological connectivity in a novel way.

1.7 Impact

The knowledge gained through a better understanding of the innate mechanisms that drive and regulate postural balance in the event of unintended perturbations was expected to meaningfully extend current research exploring the action-perception properties of affordances beyond actions associated with volitional movements. Additionally, these results were expected to have the potential to provide fundamental new insights into applications that may serve to inform best practices for fall prevention research.

2.0 FUNCTIONAL NEAR-INFRARED SPECTROSCOPY

2.1 Neuronal Metabolism

During a response to an environmental stimulus, the brain undergoes a number of

physiological changes in electrical activity and blood hemoglobin levels. These changes produce differential optical properties in the brain that can be captured through optical imaging by using light in the near-infrared range (Jobsis, 1977).

Neural activity is powered by oxidative phosphorylation, in which adenosine triphosphate (ATP) is formed due to the transfer of electrons across the electron transport chain through chemiosmosis (Hall et al., 2012). Oxidative phosphorylation is responsible for 87% of ATP generated in the neuronal cell body (Kety, 1957; Sokoloff, 1960). As a result, brain activity is dependent on the ability of vascular channels to provide cortical regions with blood that is rich in oxygen and glucose (Attwell & Laughlin, 2001). Immediately following neuronal activation, the available substrate in that region is utilized. This reduction in glucose and oxygen stimulates the brain to increase local arterial vasodilation. Subsequently, cerebral blood flow and volume increase in the region known as neurovascular coupling (Gratton et al., 2001), which is achieved due to a highly-developed network of capillaries and vessels at distances of 20-40 µm that are embedded within the cortical structures. These channels allow for blood flow to match the degree of neuronal activity in those regions (Villringer & Dirnagl, 1995; Hirase et al., 2004). As a result, there is a temporal relationship between neuronal activity and mitochondrial function, which exists as long as sufficient substrate is provided to the active tissue. It has been demonstrated that rapid calcium dependent mitochondrial NAD(P)H oxidation and oxygen consumption occurs 200 ms following purkinje neuron depolarization (Hayakawa, Nemoto, et al., 2005). These purkinje neurons are imperative in motor coordination as they send inhibitory projections to the deep cerebellar nuclei and are the single output for motor

coordination in the cerebellar cortex. This increase in blood to the area usually exceeds the amount required for neuronal oxygen utilization which produces an overabundance in the active cortical area (Fox et al., 1988). fNIRS imaging takes advantage of this overabundance of blood flow and the different hemoglobin species contained within.

2.2 Optical Histo-physiology

Oxygenated (oxy-Hb) and deoxygenated hemoglobin (deoxy-Hb) poses optical properties that are visible in the near-infrared light range. These can be used to measure changes in the ratio of their concentration during neurovascular coupling (Chance et al., 1993; Villringer & Chance, 1997). The majority of biological tissue is transparent to light in the near infrared range between 700-1000 nm due to their absorption of light being quite small (Farzin et al., 2007). The chromophores of oxy-Hb and deoxy-Hb, however are able to absorb certain wavelengths at this range known as the optical window (Jobsis, 1977). A chromophore is a region in a molecule in which light of a certain wavelength is absorbed. Specifically, it is a region in which two separate molecular orbitals possess an energy difference that is within the range of the visible spectrum. As such, a chromophore is denoted as the functional group that causes a conformational change in the structure of the molecule when hit by light energy. This light can thus be absorbed by exciting an electron from its ground state into an excited state. Oxy-Hb and deoxy-Hb species have different absorption coefficients, which relate to how likely a photon is to get absorbed as it moves through this medium. A larger absorption coefficient value mean it's more likely to get absorbed.

In this optical window, the absorption by water is relatively low and the absorption is dominated by hemoglobin. When photons are projected into the scalp by the source diode, they pass through the upper scalp and are scattered throughout the tissue. Three main types of scattering of photons in biological tissue exist: rayleigh, debye, and mie scattering. Mie scattering occurs for particles that have larger radii than λ and this is what is seen in fNIRS imaging. As these particles propagate throughout the scalp, skull, cerebrospinal fluid, and upper cortical regions, they are reflected and scattered. Some of these photons are intercepted through absorption by oxy-Hb and deoxy-Hb (Gratton et al., 1994). The photons that reflect and follow an elliptical path back to the surface of the skull are measured using the detector optode (Gratton et al., 1994). As chromophore concentration change during neurovascular coupling, so to do the intensity of the reflected light which is quantified by using a modified Beer-Lambert law, which relates the light attenuation to properties of the material in which it is travelling. This law helps to resolve the scattering of photons that are reflected by oxy-HB and deoxy-HB and passed through the scalp (Cope & Delpy, 1988; Cope, 1991).

Oxy-Hb and deoxy-Hb have an isosbestic point of 810 nm in which light absorption is identical between the two molecules. This is due to a relation in the linearity of the stoichiometry of the molecules. As a result, the relative concentration of the two chromophores can be measured by measuring absorbance/reflectance changes at two wavelengths, one which is specific to oxy-Hb and one that is specific for deoxy-Hb (Figure 1). If photons from at least two wavelengths of light are sent into the system and the change in absorption over time is assumed to be due changes in the concentration of oxy-Hb and

deoxy-Hb, then the photons are inversely proportional to the concertation of the chromophores along the optical path that was traveled. Additionally, water is assumed to be a constant background in this model.
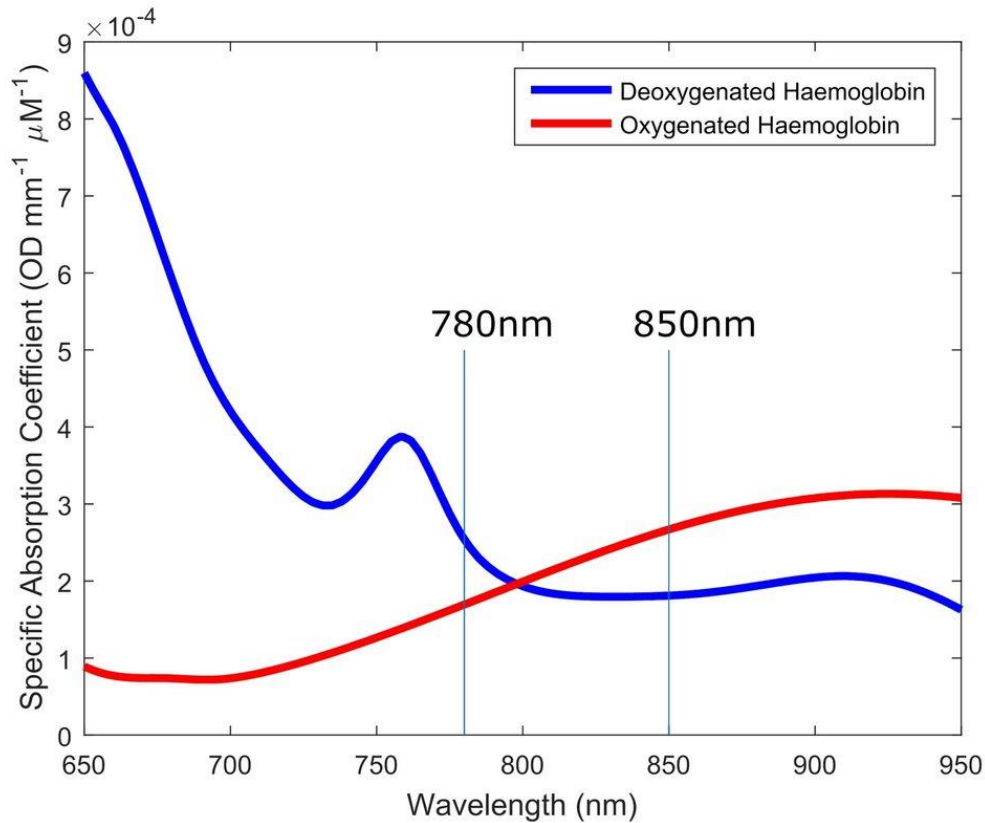
Figure 1: Graphical representation of chromophore concertation (OD mm^{-1}μM^{-1}) as a function of wavelength (nm). At an isobestic point of 810nm oxy-Hb and deoxy-Hb species experience chromophore concentration differences in the near infrared range (650-950 nm) adapted from (Farzin et al., 2007).

2.3 The Temporal Resolution of the fNIRS Signal

Arterial vasodilation and the influx of blood flow that follows cortical region activation, begins with a rapid increase in oxy-Hb, in addition to a slower, lower amplitude decrease in deoxy-Hb (Leff, et al., 2011). These changes, as well as an overall increase in hemoglobin concentration are illustrated in the fNIRS data (Figure 2). Specifically, there is

a delay of response greater than 2s between stimulus onset to hemodynamic changes. Concentration levels of Oxy-Hb and total hemoglobin typically peak within 5-10s following motor stimulation, followed by a subsequent decrease during the remainder of motor stimulation (Akiyama et al., 2006; Colier et al., 1997; Durduran et al., 2004; Hirth et al., 1997; Horovitz & Gore, 2003; Maki et al., 1995, 1996; Mehagnoul-Schipper et al., 2002; Miyai et al., 2001; Obrig et al., 1996a; Sato et al., 2006; Strangman et al., 2003; Toronov et al., 2000, 2001; Watanabe et al., 1996; Wolf et al., 2002; Leff et al., 2011). However, the time for deoxy-Hb to reach its lowest concentration is more variable and may not occur for 15s post motor stimulation onset. Generally, there is a 1-2s temporal offset between oxy-Hb and deoxy-Hb (Toronov et al., 2001; Franceschini et al., 2003; Jasdzewski et al., 2003). These times, however, are not fixed or predictable and rather depend on the chromophore concentration, the type of motor stimulation, and the duration of its onset/offset. Additionally, the rest period in between stimulations period will have an effect on subsequent trials if not performed for an appropriate amount of time. Generally, as the duration of motor stimulation increases, so to do the time to peak and time to lowest concentration for the oxy-Hb and deoxy-Hb respectively (Leff et al., 2011). Due to a general lack of reporting regrading hemodynamic recovery data it is difficult to determine a standard time. However, from the data that is available, a 10-15s period is sufficient for typical stimulation protocols (Obrig et al., 1997; Toronov et al., 2001; Boden et al., 2007; Leff et al., 2011).
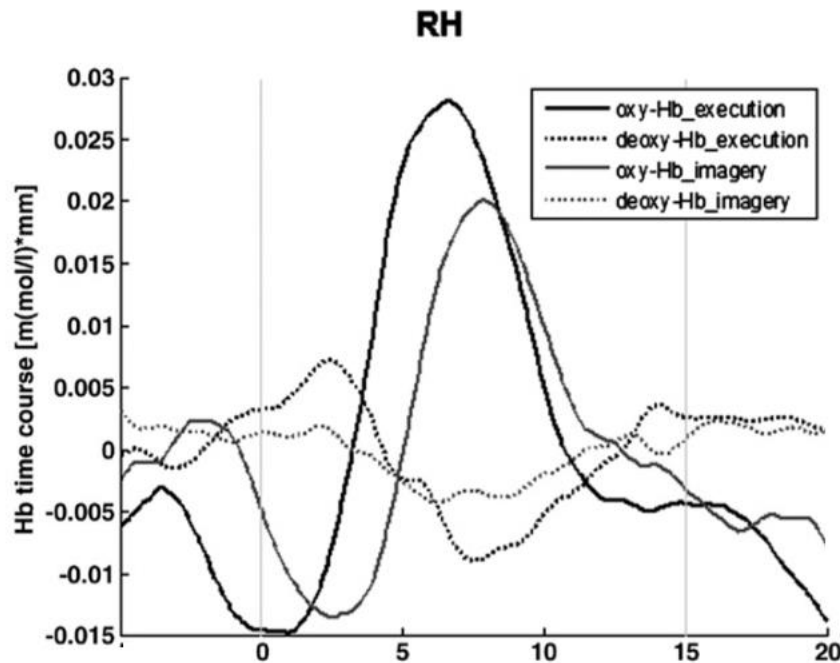
Figure 2: A typical graphical representation of changes in magnitude of oxy-Hb and deoxy-Hb concentration [m(mol/l)*mm] as a function of time (s) in the right hemisphere during an experimental trial. Stimulus duration occurs from 0 to 15s. Peak concertation increase of oxy-Hb occurs ~7s post stimulus onset. Time to nadir for deoxy-Hb occurs ~8s post stimulus onset (Wriessnegger et al., 2008).

2.4 Validity of the fNIRS System

Several comparative analyses have been performed to test the validity of the fNIRS platform relative to more established brain imaging equipment such as fMRI, currently considered the gold standard for measuring functional brain activation (Irani et al., 2007). Both are indirect measures of neuronal activity, with a temporal resolution on the order of seconds, due to the hemodynamic response that they measure. As a result, fMRI is good comparative platform to examine the validity of the fNIRS signal.

High temporal correlations between the BOLD signal in fMRI and the deoxy-Hb concentration in fNIRS during a motor task has been shown (Toronov et al., 2001).

Additionally, amplitude correspondence between the BOLD and deoxy-Hb signal were shown to be highly correlated, even when accounting for biological tissue of the scalp and skull (Strangman et al., 2002). These findings have been extended to a simple motor task, in which fNIRS and fMRI was concurrently recorded. Both measures showed significant correlation across all participants regarding the level of activity in the motor and sensory cortices (Huppert et al., 2006; Schroeter et al., 2006).

The within-subject stability of detected cortical activity with fNIRS has been tested and found to be highly reproducible across all participants in regards to the location, quantity and temporal information of the detected signal over a six-month test and re-test period (Plichta et al., 2006, Sato et al., 2006). As a result, due to the high correlation between task induced hemodynamic changes recorded by fMRI and fNIRS, the fNIRS measure technique reliably monitors brain hemodynamic changes that corresponds with functional brain activation (Mackert et al., 2008; Sander et al., 2007; Leff et al., 2011).

3.0 METHODS

3.1 Participants

Twenty-two participants (10 males, 12 females; mean age 23.8 ± 2.1 years) from the McMaster University community participated in this experiment. All participants possessed normal or corrected-to-normal vision, were free of any neurological impairment affecting cortical function or upper limb function, were free of any upper extremity disorder or injury and were right hand dominant as determined by the Edinburgh Handedness Questionnaire (Oldfield, 1971). Following participant recruitment, anthropometric measures of arm limb length and head circumference were recorded. Limb length was

calculated as the length between the acromion to the end of the third digit when the participants arm is outstretched. Limb length was used in order to ensure that the objects were presented within the graspable reach of the participant. In the current study, graspable objects were presented at a distance to the participant representative of ~75% of their arm length. Head circumference was measured in order to ensure that the *NIRSport* cap was a proper fit for the participant. This was accomplished through measuring the circumference of the head from the bridge of the nose to the inion at the base of the skull. Participants were given a pair of noise cancelling uncorded ear plugs (Uline Uncorded Earplugs, Uline, Milton, ON) to wear during the experiment to prevent them from hearing when the release pin on the chair was pulled. Participants were compensated $20 for their time.

3.2 Stimuli

Three stimuli were used in this experiment. Two of the stimuli consisted of a graspable pole that was presented in two orientations (LR orthogonal, RL orthogonal). Additionally, a flat surface was used to act as a control (C). This control stimulus did not afford any form of graspable action. Both graspable stimuli used in this experiment were constructed out of 1.5-inch outer diameter metal grasping handle that was 16 inches in length. The poles external diameter was between 32 mm to 51 mm defined as the standard for hand rail designs by the 2010 ASD standards for accessible design (United States Department of Justice, 2010). The pipe was covered in black grip tape and mounted onto a 16-inch piece of flat pine wood. A bolt was placed centrally in the wood so that it could be loosened and tightened in order to set the pole to the varying orientations outlined above. For the control condition, a 12-inch square board of plywood was centrally mounted with

the same bolt system. These objects were then mounted to a wooden support structure that kept the objects stable and could support the weight of the participants grasp. The support structure also allowed for the poles to be adjusted based on the size of the participant (i.e., the height, width and depth of the pole position could be changed). The graspable poles were positioned such that the center of each pole was in line with the participants shoulder of the respective side.

During the experimental protocol, participants were presented with two objects in front of them at all times (i.e., one on their left and one on their right side). Therefore, there are nine possible combinations with the objects outlined above (LR LR, LR RL, LR C, RL LR, RL RL, RL C, C LR, C RL, C C) (Figure 3). These stimuli were presented twice and each object was presented on each side six times. Additionally, two catch trials were included in which a posterior tilt perturbation was not delivered. This arrangement thus resulted in 20 experimental trials to comprise part 1 of the experiment. Throughout these trials, hemodynamic changes in the right and left pre-motor cortices, during a visual preparatory period of 15±5s prior to perturbation onset, were measured using a continuous wave functional near infrared spectroscopy system (*NIRSport,* NIRX Medizintechnik, Germany). Following these 20 experimental trials, an additional 10 trials were performed in which participants experienced the posterior tilt perturbation but did not receive vision until the moment of perturbation onset (part 2 of the experiment). For this part, each stimulus combination pair was presented once (n=9), in addition to one catch trial. The order of these stimulus combinations was randomized for each participant. fNIRS data was not collected due to the short temporal window of stimulus presentation.
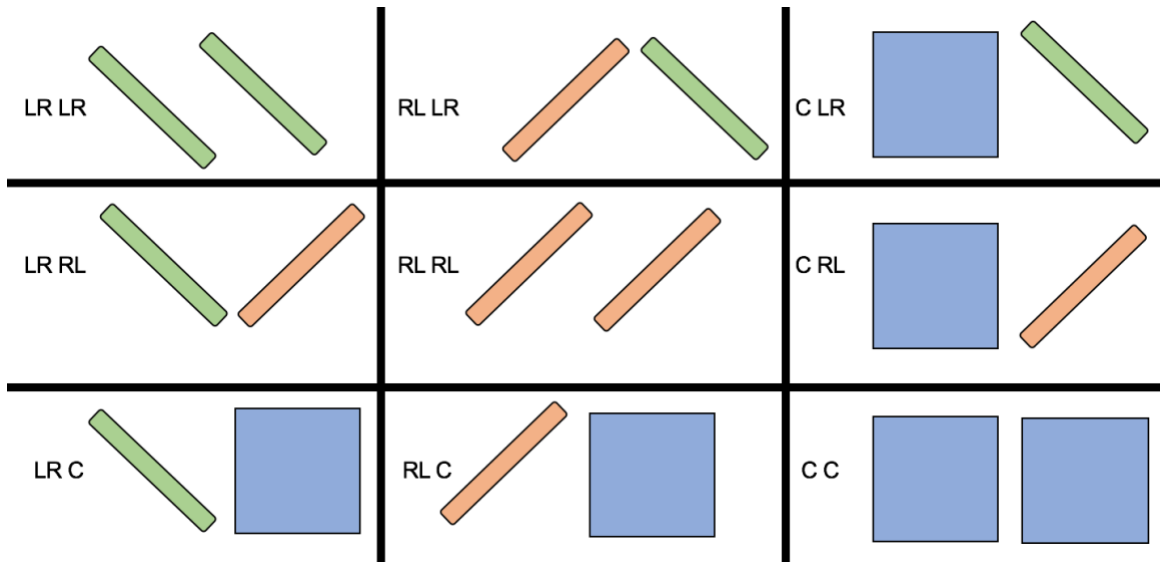
Figure 3: Two-dimensional representation of the nine stimulus combinations used in this experiment.

3.3 Apparatus

Performing a whole-body perturbation allows the system to use compensatory strategies involving both the lower limb and upper limb. As the purpose of this study was to determine the cortical contributions to graspable objects, perturbations were restricted such that upper-limb prehension was the only compensatory strategy that could be used. As a result, participants were seated in a custom-designed chair that delivered whole-body perturbations by posteriorly tilting 30° in the sagittal plane (Figure 4). Participant's feet were resting on an elevated platform such that their knees were bent at ~90°.

The chair was mounted onto a hinge that provided the 30° posterior tilt (i.e., the maximum tilt that the hinge would allow the chair to traverse). Posterior tilts were caused by a weighted cable that was attached to the top of the chair. Once a mechanical release pin was pulled from the hinge, the chair was pulled posteriorly by the weight of the attached

cable. The chair was stopped by foam safety pads mounted on the rear of the structural base, that prevented the participant from experiencing a large deceleration or jerking movement when the chair reached the maximum tilt angle of 30°. An *arduino prototyping platform board* (Mouser Electronics, Tex, United States) was mounted on the top of the chair to measure the time between the start and end of the perturbation. A goniometer was used to measure the angle and distance of the posterior tilt experienced by the chair. Velocity and acceleration were calculated using the data obtained from these devices and was found to be between $0.69 \, \text{m/s}^2$ (chair only) and $1.84 \, \text{m/s}^2$ (person in the chair). These accelerations were consistent with previous research, which delivered perturbations at an acceleration of 1-2 m/s^2 (King et al., 2010; Sarraf et al, 2014). Participants were strapped into the chair with a belt over their trunk and waist to prevent lateral translation of their body during the tilt. These belts did not impede their ability to make upper body corrective movements with their arms. Participants' head was placed on a padded head rest that cushioned their head and neck during the deceleration phase of the perturbation. Additionally, the participants were able to lean the back of their head against the pad when the chair was upright thereby preventing excessive movement of the fNIRS cap and reducing strain of the participants neck to keep their head upright. Similar apparatuses have been used in other fall research involving grasping (Van Ooteghem et al., 2013; Gage et al., 2007; Akram et al., 2013).
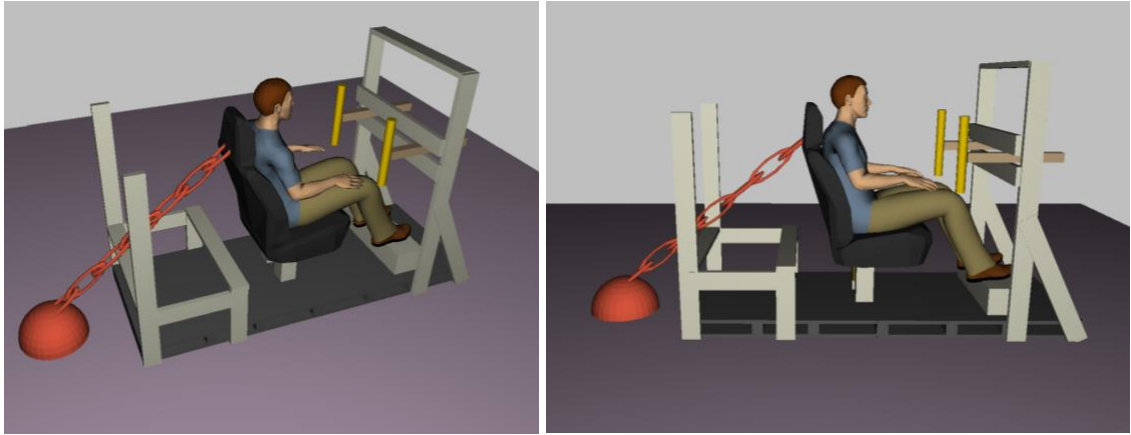
Figure 4: Depiction of the apparatus. The chair was mounted on an axis of rotation such that a posterior translation (30°) from the starting position could be delivered. The orange chain represents the weighted cable and the two graspable poles are displayed in yellow.

3.4 Video Recording

A *GoPro Hero 3* camera was mounted facing the participants above the rigging that supported the graspable objects. This allowed for video recording of the upper-limb compensatory reactions that participants performed in response to the perturbation. These data were used in order to assess the behavioral compensatory reach-to-grasp actions executed by the participants.

3.5 Assessing Motor Activity

In order to measure hemodynamic changes in the right and left premotor and motor cortices (M1), a multi-channel continuous wave imaging system *NIRSport* (NIRX Medizintechnik) was used at a sampling rate of 7.81 Hz. This is a continuous wave fNIRS system in which light is emitted from the optode at a constant amplitude and measurement is achieved through attenuation of the reflected light. The intensity of light applied to the sample remains constant and the intensity of light that comes out is measured continuously.

This process allows for a greater temporal resolution to capture dynamic changes in the brains histophysiology compared to other fNIRS imaging systems. (Hoshi, 2003; Izzetoglu et al., 2004; Obrig & Villringer, 2003). This application also provides advantages over other fNIRS platforms as LED optodes are used, rather than lasers, making testing safer with respect to the eyes. Additionally, the equipment is portable and is able to be stored in a backpack to allow for ecological applications in the testing of participants in operational environments (Izzetoglu et al., 2004).

The system uses near-infrared light at two wavelengths (760 nm and 850 nm) in order to detect concentration changes in deoxy-Hb and oxy-Hb respectively. The detector and source optodes were set 3 cm apart. This allowed activity to be measured from the top 2-3 mm of the cortex (as well as 1 cm lateral on either side perpendicular to the axis of the source and detector optode spacing) (Chance et al., 1988; Tamura et al., 1997; Firbank et al., 1998). This measurement depth allowed for detection of hemoglobin concentration changes in the grey matter, which is where information integration is suggested to take place (Herrera-Vega et al., 2017).

Two 4x4 source-detector sets consisting of 4 source and 4 detector optodes each were used in order to measure hemodynamic changes in premotor cortex in the right and left hemisphere, in response to object orientation prior to a perturbation. The sensing geometry of this montage was registered to a human atlas using a *NIRSite* (NIRX Medizintechnik) computer application. This application provides the x, y and z position coordinates of each optode. This system, however, does not account for the stretch of the fNIRS cap over a participant's head and the shift in position of the optodes that may occur.

As a result, these coordinates were cross checked using neuronavigation, which allows for a more realistic depiction of the optode positions by having a research assistant sit upright in a chair while wearing the fNIRS cap without any source detectors attached. *Brainsight neuronavigation* (Rogue Research) was then used to determine the x, y and z coordinates of each of the source detector optode holders. The resulting coordinates were compared with those determined from NIRSite. Due to these caps being a relative system, these coordinates should be comparable across all participants. Detectors 3 and 7 were positioned over C3 and C4 respectively. A 3-dimensional atlas (Collin-27 brain template) was then registered with these coordinates using *AtlasViewer* software (National Institutes of Health) (Collin et al., 1994). The program projects topographical data based on skull landmarks associated with the 10-20-system. The reference points for this Atlas were set with the landmarks cz, nz, rpa, lpa, and iz. This allowed the atlas to be registered to the dimensions of the participant's head, thus allowing for a more accurate depiction of the source detector positions. Once the source-detector optodes were registered using the x, y and z coordinates, the 20 recording channels were added and projected onto the cortical surface of the atlas. This produced the specific coordinates of the cortical surfaces measured by each channel using the Montreal Neurological Institute (MNI) coordinate system. These coordinates are subject to inter-individual variability; however, this procedure allows for the most probabilistic reference to cortical areas of the brain surface underlying the channels for this study (Hofmann et al., 2008). These coordinates were then inputted into *BioImage Suite* to determine the respective cortical region measured by each channel.

BioImage Suite uses the Colin brain atlas to map MNI coordinates using a *BioImage Suite* derived tracing tool (Organization for human brain mapping, 2008).

3.6 Motor Cortex Sensing Geometry

The international 10-20 system was used in order to locate M1 in the right and left hemisphere of participants (Figure 5). This was accomplished by measuring the distance between the nasion and inion, as well as the left pre-ocular point and right pre-ocular point. The nasion is a depressed area located in between the eyes and is just above the bridge of the nose, while the inion is the crest at the back of the skull. The pre-ocular points are a cartilage projection from the pinna of the ear. Once these values were recorded, the Cz point (middle of the head) was determined by calculating the midpoint between the two measures previously stated. Once Cz was located, C3 (representative of M1 of the left hemisphere) was determined by calculating 20% of the distance between the right and left pre-ocular points. This value was then used to measure a line perpendicular from Cz to the left pre-ocular point. The end of this line represented C3. The same procedure was used to identify C4 (representative of M1 of the right hemisphere) using the right pre-ocular point. These values were used to ensure that detector 3 and 7 were positioned over M1 of the left and right hemisphere respectively for each participant. This increased the reliability of the cortical detecting space for each participant.
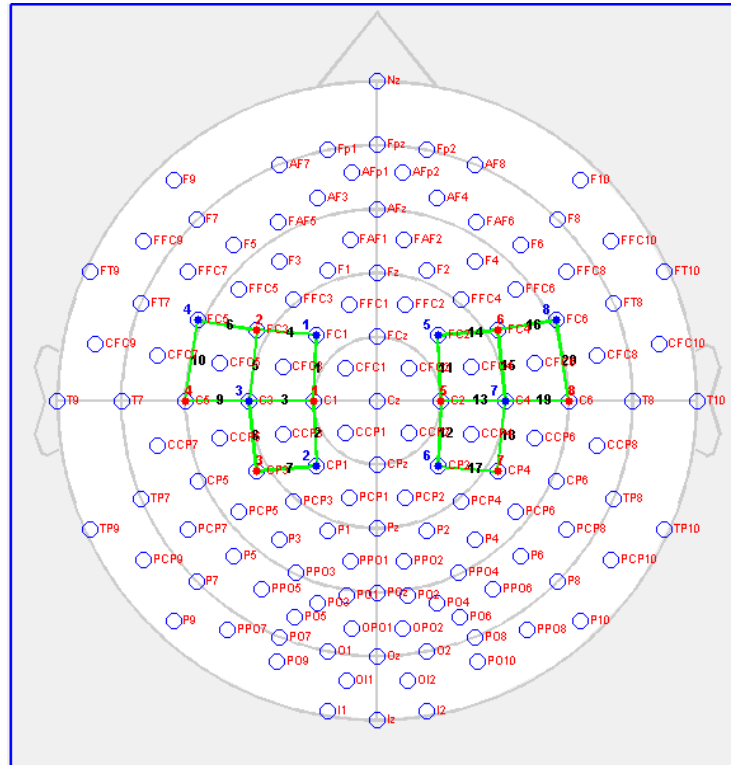
Figure 5: Cortical region representation using the international 10-20 system. C3 and C4 estimates the spatial location of the left and right primary motor cortex respectively.

3.7 Protocol

3.7.1 Dark Noise Test

Prior to participants entering the lab, a dark noise test was performed on the NIRS equipment. Dark noise is produced by a photo-detector when there is complete shielding from all external optical radiation and voltages are applied to the photo-detector and it is indicative of those used during experimental operation (Desai & Valentino, 2011). This is performed in order to assess the level of noise that is inherent in the fNIRS system, as excessive noise can compromise the quality of the data (Muhogora, et al., 2011).

Specifically, the noise level across each detector was checked to be near the same value under 1.5 mV, with a gain of 0.

3.7.2 Calibration

The fNIRS cap was populated with the source detector pairs and placed on the participant's head using spring tension caps as well as a zipper "over cap" that added pressure to the optodes. Each channel was then inspected for hair that could interfere with the connection between the sour/detector and the scalp. If hair was present, it was carefully removed from the area with a *Q-tip*. Calibration was then performed to check that each source and detector pair were communicating and that the signal was not impeded by hair that might have been missed during the first removal. Additionally, during calibration, the instrument determined the optimal gain for each of the source detector pairs. The gain levels were numbered from 0 to 2 with a 10-fold amplification factor applied with each level. The gain was evaluated through the calculated mean from 4 scans for each amplification level and considered optimal if the raw signal from a channel fell between 0.4V and 4.0V. During this time, the quality of the signal was updated to reflect the gain settings as well as noise apparent in the signal. Three levels of data quality were identified by the system for each channel. Green= Good, Yellow= Acceptable, Red= Reject (hair between the optode and the scalp can impede the ability for source detector communication and thus the data quality). Data collection was only performed if all channels were green. If a channel appeared yellow or red, the corresponding source detector pair for that channel was identified and further hair removal was performed.

3.7.3 Acquisition of Experimental Trial

3.7.3.1 Part 1 Baseline

Participants wore safety goggles covered in black electrical tape to block their visions when the graspable objects were set up before each trial. During this time, participants were seated comfortably with their arms relaxed and their hands resting on their thighs with their palms down. This time (~2.5 minutes) allowed for hemodynamic changes incurred due to previous activity to return to a resting level. It has been shown that a 10-15s rest period is sufficient for typical stimulation protocols (Obrig et al., 1997; Toronov et al., 2001; Boden et al., 2007; Leff et al., 2011). Due to the intense nature of the perturbation stimulus however, 2.5 minutes were provided. Once the 2.5 minutes had elapsed, a 30s baseline fNIRS measurement was recorded. Participants continued to wear the safety googles during this time and were instructed to sit as still as possible and relax.

A baseline measurement was recorded prior to each trial as each recording during the experimental trial was averaged to the preceding baseline in order to capture increases in the cardiac cycle that may occur over successive trials that was not recovered during the 2.5-minute rest. This was accomplished by subtracting the average of the baseline from all data points of the stimuli trace. Additionally, as fNIRS measures relative hemodynamic changes in the cortex, the baseline was used to act as a reference value to which all other changes during the stimuli protocol were compared to. As such, any increases or decrease in hemoglobin species as a result of the stimuli were relative to the previous baseline.

3.7.3.2 Part 1 Experimental Trials

A trial began with a baseline recording. Following the 30s, the goggles were carefully removed by a research assistant, thus revealing both objects to the participant. At this point, the participant was able to view the objects for a period of 15s. Participants were instructed to only shift their gaze and to keep their head as still as possible. Based on previous literature, 15s is sufficient time for the hemodynamic response to reach a peak for that trial (Akiyama et al., 2006; Colier et al., 1997; Durduran et al., 2004; Hirth et al., 1997; Horovitz & Gore, 2003; Leff et al., 2011; Mackert et al., 2008; Maki et al., 1995, 1996; Mehagnoul-Schipper et al., 2002; Miyai et al., 2001; Obrig et al., 1996a; Strangman et al., 2003; Toronov et al., 2000, 2001; Watanabe et al., 1996; Wolf et al., 2002;). Once the 15s had elapsed, a variable foreperiod (0-5s) began in which participants experienced a fall during non-catch trials. Participants were instructed, that when the perturbation was initiated, to respond by grasping an object with whichever arm they choose, in order to prevent themselves from falling backwards. If they chose to respond with their right arm, they were required to reach out for the right object. The same was true for the left. This was required to preserve the compatibility nature of the two graspable stimuli. fNIRS recording occurred concurrently throughout the entire trial and was ended 10s after the tilt. Once the fall had occurred, participants were pushed back into position and the chair was locked at the original vertical orientation. The safety googles were placed back on the participant and they were given a 2.5-minute break, while the researcher prepared the next set of stimuli. This protocol was repeated for the 20 experimental trials.

3.7.3.3 Part 2 Experimental Trials

During part of the experimental protocol, 10 trials were performed in which participants wore a pair of *PLATO visual occlusion spectacles* (Translucent Technologies Inc., Milgram, 1987). fNIRS recording was not performed during this part of the experiment. Participants sat in the same chair in the same position as outlined in Part 1. Participants sat with the occlusion spectacles closed so that they could not see the objects in front of them. Once the objects were set up, participants sat in the chair for a variable foreperiod (0-15s) in which a posterior tilt occurred. The occlusion spectacles opened to reveal the two objects at the moment that the posterior tilt was initiated. Participants were asked to reach out in the same manner as described in Part 1, to mitigate the posterior tilt. Behavioral reaching responses were recorded via a video camera.

3.8 fNIRS Data Processing

The forward model was used to describe the physics of how light shined through the scalp propagates down into the head. A fundamental principal of this model is that the absorption coefficient of water in the optical window is low and the scattering of light by the tissue is quite high. This allows for inferences to be made regarding the spread of the photons into the scalp and focuses the absorption as a result of hemodynamic species in the blood. As a result, the goal of the analysis, and processing of the fNIRS data, was to isolate the hemodynamic changes occurring in the vascular network of the grey matter which is primarily achieved through filtering and discretization.

Hemodynamic optically measured evoked response (HomER2) (National Institutes of Health) is a Matlab based graphical user interface that was employed for the functional

analysis of the fNIRS data. This program allows users to customize the data analysis to reflect the experiment, such as NIRS probe sensing geometry, the optical wavelength used, and the stimulus design. The program allows for three levels of data processing dependent on the data inputted. The third level was used for the purpose of this study as it allows for processing of multisession group data as well as the averaging from multiple participants across multiple trials. The individual participant trials were first processed separately and then averaged together in order to produce average responses for a trial for a selected region of interest (left or right hemisphere). Additionally, individual computed hemodynamic response functions (HRF) were used for statistical analysis.

3.8.1 Processing Stream

The raw data was uploaded into Homer2 and HRF's were generated through a custom eight-part processing stream. Prior to filtering, the raw data were converted to changes in optical density using the modified Beer–Lambert law. Motion artifacts (MA) were then identified using the *hmrMotionArtifact-ByChannel* function. This function identifies MA's on a channel by channel basis using a predetermined set of thresholds related to the changes in standard deviation of the data (STDthreh) or in absolute signal amplitude (AMPthresh). A specified period of time (tMotion) was set during which the changes are examined. If a MA is identified, the program marks a specified time range around it (tMask) in red (the values used in this study were AMPthresh = 1, STDthresh = 10, tMotion = 0.5s and tMask = 1s). These values were used because they provide a more conservative estimate of MA's. As large spikes were not expected due to the experimental protocol, the MA identification was created to be more sensitive to smaller movements that

may impact the signal. Once MA's were identified, a target principal component analysis (tPCA) was run (*hmrMotionCorrectPCArecurse*). This function creates a matrix of measurements, where the data is arranged as a number of time points by a number of channels. This matrix was then transformed into a set of orthogonal vectors in decreasing order based on the amount of variance present. The main assumption that underlies this process is that an MA, if to occur, would be equally present in all channels. This MA would also possess a similar temporal variation among these channels and account for the majority of variation. This function was performed solely on the 1s of data that was previously identified as containing a MA using the *hmrMotionArtifact-ByChannel* fucntion. Once the segment of time possessing the MA was identified, an N_{tPCA} number of components are then projected out of the data to account for 97% of the variance. The epochs of corrected motion are then brought back together (the values used in this study were AMPthresh = 1, STDthresh = 10, tMotion = 0.5 s and tMask = 1 s, Nsv= 0.97). These values were set in order to match the MA identification function.

The *hmrMotionArtifact-ByChannel* function was then re-run in order to identify any residual MA's that were not corrected by the tPCA. The same values were used at outlined above. If the data still possessed an MA, all channels from that trial were removed using the *enStimRejection* function. The data were then band-pass filtered with a low pass set at 0.5 and high pass set at 0.02 Hz. This was performed in order to remove low-frequency drifts and high-frequency noise such as cardiac pulsation. Finally, the filtered optical density data was then converted to hemoglobin concentration and blocked averaged using the *hmrBlockAvg* function. As such, the mean of the baseline data were subtracted from

each data point during the stimulus window. This produced the relive concentration changes in oxy-Hb and deoxy-Hb for each channel. The time range (trange) was set at -25s (representative of the bassline measure) and +13s (representative of the stimulus data). These values were used rather than the full 30s baseline and 15s stimulus period in order to account for potential timing errors during the experimental protocol. These errors could have manifested as a result of a miss communication between the researcher and the research assistant in terms of removing the goggles after baseline or initiating the perturbation too early.

3.9 Statistical Analysis

3.9.1 Behavioral Data Part 1

The behavioral results for part 1 of the experimental protocol was computed based on the responses made towards a set of stimulus combinations. Reponses were defined as either a catch, miss, or flinch (the latter being defined as a motion of the limb without the hand leaving contact with the thigh) with either the right, left or both hands, as well as no response. The proportion of each response was calculated and graphed. From the numerical data, each type of response was collapsed such that a right catch, right miss, or right flinch all represented a right-hand response. The same was performed for the left hand. Grasping actions made with both hands were removed from the data as errors, as participants were instructed to only respond with one hand. The stimulus combinations were then defined based on their ability to afford a grasping action to either for the left or right hand (Table 1).

Stimulus Combination	Compatibility
LR LR	Right
LR RL	None
LR C	Left
RL LR	Both
RL RL	Left
RL C	Left
C LR	Right
C RL	Right
C C	None

Table 1: The compatibility of each stimulus set for a right hand/ left hand grasp.

The stimulus combinations LR RL and C C were excluded from the data set as they did not represent compatible grasps for either the left or the right hand. In addition, RL LR provided equally optimal grasping opportunities for both the left and right hand and, as such, the number of responses made by each hand were considered separately. These values were then computed using a Pearson's 2x2 chi-squared test for independence, with the factors of hand of response (right or left) and object optimality (right hand or left hand). The null hypothesis for this test was set to assume that no association between the two categorical variables existed. Adjusted Pearson's residuals were used for post hoc testing and were calculated based on the following equation (Eq. 1).

$$r_{(\text{Adj})ij} = \frac{O_{ij} - E_{ij}}{\sqrt{E_{ij}(1 - \frac{m_i}{N})(1 - \frac{n_j}{N})}} \qquad (1)$$

Where $O_{ij} - E_{ij}$ are the residuals, m_i is the row total, n_j is the column total and N is the total number of observations. A Pearson residual whose absolute value was greater than 2 was set to represent a significant deviation from expectancy.

3.9.2 Behavioral Data Part 2

The same process as outlined above was conducted on the behavioral responses for part 2 of the experimental protocol.

3.9.3 fNIRS Data

Continuous wave fNIRS systems work by measuring hemodynamic changes relative to a baseline. These values do not correspond to the exact amount of hemoglobin species present in the detected grey matter, but rather represent a relative increase or decrease in response to a stimulus. Sample based statistical tests are limited in terms of their ability to utilize the time course of the data. As a result, modeling the NIRS data is based on an assumption of linear addition of hemodynamic changes over time in order to assess these changes in response to stimuli. The effects of the hemodynamic change were added in order to form the measured signal change (Eq. 2) (Huppert et al., 2009).

$$Y = U_{stim} \otimes \beta + e \tag{2}$$

In this equation, Y represents the recorded time series of the observation of the hemodynamic variable, β represents the parameter vector that is being solved, $\otimes$ represents the convolution of the regression variable (timing of stimuli) with the impulse response to that regressor (hemodynamic response) and e represents the error term which is assumed to be normally distributed, zero-mean, random noise. In order to estimate the mean effect of each of the individual functional responses, a deconvolution of Eq. 1 was performed, allowing the construction of a full-time course of the evoked response by estimating each point independently. This produced the shape of the evoked response, with the temporal window of interest being the duration of a single trial (13s). Through this, an *a priori* assumption was made regarding the temporal shape of the hemodynamic response. Specifically, a canonical temporal basis set models the response as a combination of one or more Gaussian functions (Boas et al., 2004; Gibson et al., 2005; Gratton et al., 2005; Huppert et al., 2009). The assumption, therefore, is that the evoked hemodynamic response can be modeled as a linear combination of these functions. This allowed the evoked response to be reduced into numerical values that could be used for statistical analysis, ultimately allowing for comparisons in the magnitude of hemoglobin concentration changes over time. Canonical based models have been shown to improve the contrast-to-noise ratio of the hemodynamic response (Toronov et al., 2000; Zhang et al., 2005; Schroeter et al., 2004).

As stated earlier, participants were given a minimum of 15s to observe the objects

prior to the perturbation. This window of stimulation was reduced to 13s for the purpose of analysis. As such, the concertation changes of hemoglobin over the 13s was baseline corrected by removing the mean activity in the interval of 25s prior to stimulus onset. It was expected that the 13s window will contain the peak concentration change in oxy-Hb, which typically occurs between 5-10s post stimulus onset (Akiyama et al., 2006; Colier et al., 1997; Durduran et al., 2004; Hirth et al., 1997; Horovitz & Gore, 2003; Leff et al., 2011; Mackert et al., 2008; Maki et al., 1995, 1996; Mehagnoul-Schipper et al., 2002; Miyai et al., 2001; Obrig et al., 1996a; Strangman et al., 2003; Toronov et al., 2000, 2001; Watanabe et al., 1996; Wolf et al., 2002). Once the data were processed at the group level (stage 3), all channels for each condition were numerically checked to determine the specific time of peak oxy-Hb amplitude. HRF inspection on each channel for each condition was then performed. Neural activity typically leads to an increase in oxy-Hb and a decrease in deoxy-Hb with these relative changes then used as a visual marker for the presence of an HRF. Once visual inspection suggested a potential channel, the presence of an HRF was numerically checked by determining if a two-fold increase in oxy-Hb occurred (Obrig & Villringer, 2003; Strangman et al., 2002).

Oxy-Hb was principally used as a marker of activation, as previous findings have shown that oxy-Hb is more temporally sensitive to concentration changes in relation to motor stimuli, whereas deoxy-Hb is more sensitive to physiological noise (Toronov et al., 2001; Miyai et al., 2001; Franceschini et al., 2003; Jasdzewski et al., 2003; Suzuki et al., 2004). The mean concentration change of oxy-Hb during the 13s-stimulus period was calculated in channels 4, 5, 6 and 14, 15, 16 representative of the left right hemisphere

respectively. This was performed for each participant in response to each stimulus condition and averaged across repeated trials.

Pairwise comparisons were set prior to data collection based on assumptions of where the HRF was most likely to occur if hemodynamic changes were mediated by the presence of graspable and non-graspable objects. Three levels of comparisons were thus set thereby allowing for a few scientifically valid comparisons that assessed the effect of contrasting combinations of object graspability and optimality, and avoided arbitrary comparisons between unrelated objects. These comparisons were performed on channels believed to be representative of the localization of oxy-Hb changes in response to the stimuli set. All analyses were conducted using a repeated-measures ANOVA with an alpha value set at .05, Greenhouse-Geisser Correction for sphericity, and Tukey's *HSD* post hoc analysis to further decompose main effects and interactions. Optimality was predefined for each object combination set based on the amount of movement of the wrist required to grasp the object. Optimality in this experiment was relative to the object orientations used. Specifically, object combinations that were defined as relatively less optimal required greater amounts of pronation or supination of the wrist to grasp.

The first pairwise comparison was conducted in order to assess the effect of having only one object that afforded a grasp. Additionally, the relative optimality of the graspable object was assessed. Specifically, RL C and LR C both presented the graspable object on the left side of the body, however, RL C was more optimal for a left-hand grasp relative to LR C. Similarly, C RL and C LR were both graspable by the right hand, however, C LR is more optimal relative to C RL. These were compared to the non-graspable stimulus set (C

C). A 5x6 repeated measures ANOVA with the independent factors of object (RL C, C RL, LR C, C LR, C C) and channel (4, 5 ,6, 14, 15, 16) was performed.

The second pairwise comparison was conducted to assess the effect of two sets of graspable stimuli where only one of the objects for each was optimal for grasping (LR LR and RL RL), compared to the non-graspable stimulus set (C C). In this comparison, although both sets of objects are graspable, LR LR was relatively more optimal for a right-hand grasp and RL RL was relatively more optimal for a left-hand grasp. This comparison was performed to determine the strength of the optimality effect of only one object per stimulus set. A 3x6 repeated measures ANOVA with the independent factors of object (RL RL, LR LR, C C) and channel (4, 5, 6, 14, 15, 16) was performed.

The third pairwise comparison was conducted to assess different sets of graspable objects that varied in terms of their relative optimality in affording a left and right hand grasp. Two stimulus sets consisting of two graspable objects each (LR RL and RL LR) were compared to the non-graspable stimulus set (C C). Specifically, LR RL and RL LR can be grasped with the left and right hand, however, RL LR was more optimal to grasp with the left and right, hand respectively, relative to LR RL. A 3x6 repeated measures ANOVA with the independent factors of object (RL LR, LR RL, C C) and channel (4, 5, 6, 14, 15, 16) was performed.

4.0 RESULTS

4.1 Positon Coordinates

The x, y, and z coordinates obtained through NirSite and AtlasViewer were recorded and the location variation between the two for each optode was calculated. The

x coordinates were fairly similar across systems, while the y and z possessed higher levels

of variation. Specifically, the mean standard deviation of the x, y, and z coordinates

across all optodes were 4.2 mm, 15.8 mm, and 27.7 mm, respectively (see Table 2).

Optode	NIRSite			AtlasViewer			Standard Deviation		
	x	y	z	x	y	z	x	y	z
nz	2.2	86.5	-49.7	0.4	85.9	-47.6	1.3	0.4	1.5
iz	-1.8	-110.7	-54.7	0.2	-120.5	-25.8	1.4	6.9	20.5
rpa	79.7	-7.2	-90.7	83.9	-16.6	-56.7	3.0	6.6	24.1
lpa	-78.3	-7.2	-90.7	-83.8	-18.6	-57.2	3.9	8.1	23.7
cz	-2.8	-15.2	47.7	-0.5	-8.4	101.4	1.6	4.8	38.0
S1	-33.8	-41.2	37.3	-39.8	-9.5	89.9	4.2	22.4	37.2
S2	-54.8	-7.2	21.1	-63.1	23.9	52.7	5.9	22.0	22.3
S3	-60.4	-69.2	14.3	-69.3	-48	65.7	6.3	15.0	36.4
S4	-80.2	-26.2	-7.7	-84.1	-13.8	24.8	2.7	8.8	23.0
S5	25.2	-41.2	38.7	38.7	-8.6	90.3	9.6	23.1	36.5
S6	57.2	-6.2	21.6	62.3	25	53.1	3.6	22.1	22.3
S7	53.0	-72.2	14.3	69	-46.9	66.4	11.3	17.9	36.9
S8	82.0	-31.2	-7.7	83.7	-11.8	25.5	1.2	13.7	23.5
D1	-32.8	-10.2	38.2	-36	27.6	77.8	2.2	26.7	28.0
D2	-33.8	-72.2	29.8	-39.4	-48.3	92.8	3.9	16.9	44.5
D3	-66.2	-39.2	16.3	-70.6	-11.5	63.1	3.1	19.6	33.1
D4	-73.8	-4.2	-4.7	-77.4	19	18.9	2.5	16.4	16.7
D5	31.0	-11.2	39.3	35.2	28.3	78	3.0	27.9	27.4
D6	26.2	-70.2	31.3	38.8	-47.7	93.2	8.9	15.9	43.8
D7	58.2	-39.2	23.9	69.7	-9.8	63.6	8.2	20.8	28.1
D8	76.6	-2.2	-1.7	77	20.4	19.5	0.3	16.0	15.0

Table 2: The x, y and z coordinates (mm) determined from NIRSite and AtlasViewer. The first column represents the optode label (S1-S8, D1-D8) as well as the 5 reference locations (nz, iz, rpa, lpa, cz) used to register the atlas to the shape of the head. The subsequent 6 columns represent the x, y and z coordinates obtained through NIRSite and AtlasViewer respectively. The last 3 columns illustrate the standard deviation between each coordinate for each optode.

Channels 4, 5, 6, 14, 15 and 16 were of particular interest for the analysis of the fNIRS data. Using the MNI coordinates from *AtlasViewer* and inputting them into *BioImage Suite,* the specific cortical location representative of each of the 6 channels was determined. Specifically, channels 4/6 and 14/16 were positioned over left and right Brodmann Area 6 (BA6) respectively, while channels 5/15 were positioned over the left and right primary somatosensory cortex respectively.

4.2 Behavioral Results Part 1

In the sample of 22 participants, the chi-squared test revealed that there was a significant association between response hand and object compatibility (X^2= 99.52, *df*=1, *p* <0.00001). When examining all possible combinations of response hand and object compatibility using the adjusted Pearson's residuals test, it was found that participants making a right response to a right compatible object and a left response to a left compatible object were observed to occur significantly more than expected (9.98). By contrast, participants making a left response to a right compatible object and a right response to a left compatible object were observed significantly less than expected (-9.98) (Figure 6).

4.3 Behavioral Results Part 2

In the sample of 22 participants the chi-squared test revealed that there is a significant association between response hand and object compatibility (X^2= 6.54, *df*=1, *p* =0.010572). When examining all possible combinations of response hand and object compatibility using the adjusted Pearson's residuals test, it was found that participants making a right response to a right compatible object and a left response to a left compatible object were observed to occur significantly more than expected (2.58). By contrast

participants making a left response to a right compatible object and a right response to a left compatible object were observed significantly less than expected (-2.58) (figure 6).
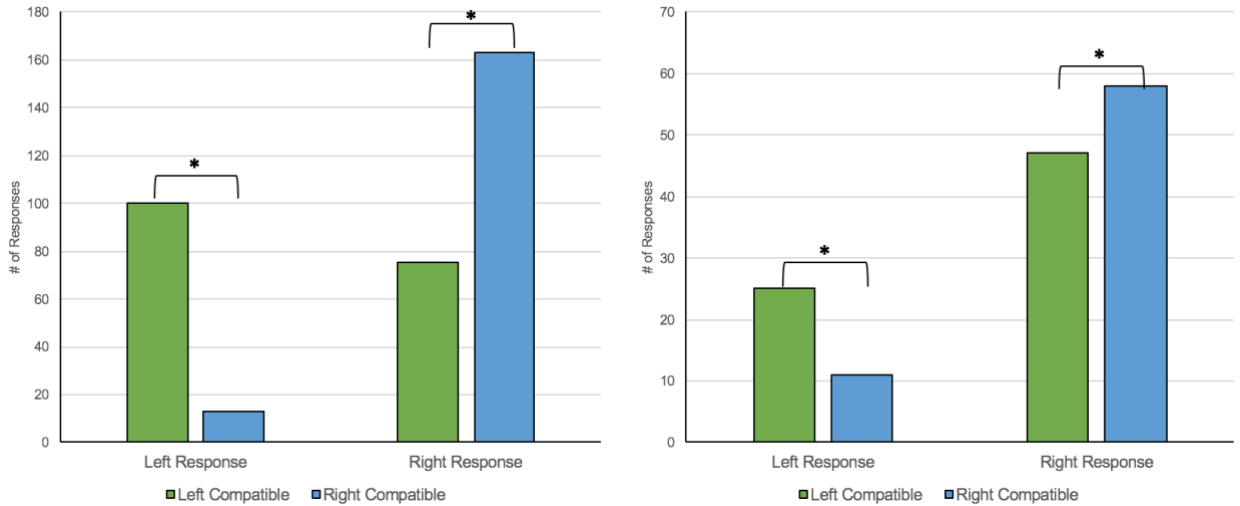
Figure 6: Total number of responses made by either the left or right hand to a left compatible or right compatible object for part 1 (left graph) and part 2 (right graph) of the experiment. *Significant difference at $p < 0.05$.
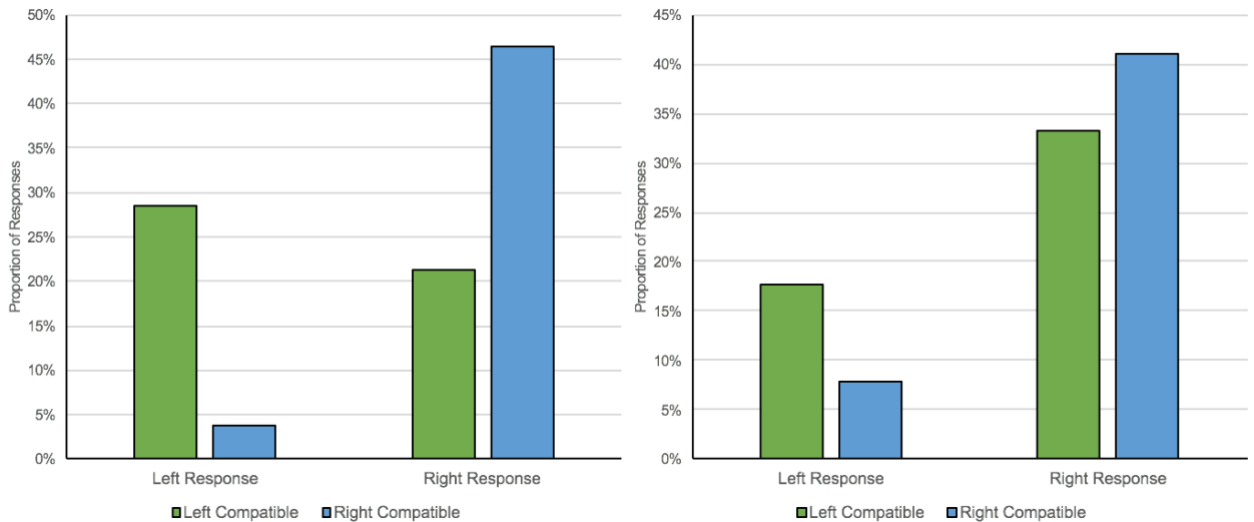
Figure 7: Proportion of responses made by either the left or right hand to a left compatible or right compatible object for part 1 (left graph) and part 2 (right graph) of the experiment.

4.4 Global blood oxygenation

Across all trials, oxy-Hb peaked within the 13s-stimulus period. Specifically, average time to peak amplitude for oxy-Hb for each condition averaged across channels (4, 5, 6, 14, 15, 16) were RL RL=4s, C LR=4s, C RL= 2s, RL C= 5s, LR C= 3s, LR LR= 3s, C C= 2s, LR RL= 5s, and RL LR= 4s.

4.5 fNIRS Results

In the first comparison, no significant interaction was found ($F_{2,21}$= 1.63, *p*=0.19, $\eta_P^2 = .07$). Mean concentration increase in the right and left hemisphere across all channels for RL C and C LR was 0.003 µM and 0.022 µM, respectively. The mean concentration change in response to LR C and C RL were -0.033 µM and -0.001 µM respectively. The mean concertation change in response to C C was -0.051 µM (Figure 8).

Figure 8: Mean concentration change in oxy-Hb across the 13s-stimulus period in response to the C RL, LR C, C LR, RL C and C C stimulus sets. All data were averaged across all participants and standard error values are reported.

In the second comparison, no significant interaction was revealed ($F_{2,21}$= 1.75, p=.186, $\eta^2_P = $ .08). Mean concentration increase in the right and left hemisphere across all channels for RL RL was 0.018 µM. The mean concentration change in response to C C and LR LR were -0.051 µM and -0.003 µM, respectively (Figure 9).

Figure 9: Mean concentration change in oxy-Hb across the 13s-stimulus period in response to the RL RL, LR LR and C C stimulus sets. All data were averaged across all participants and standard error values are reported.

In the third comparison, no significant interaction was revealed ($F_{2,21}$= 2.29, p=.114, $\eta_P^2 = $. 1). Mean concentration increase in the right and left hemisphere across all channels for RL LR was 0.023 µM. The mean concentration change in response to C C and LR RL were -.051 µM and -0.004 µM, respectively (Figure 10).
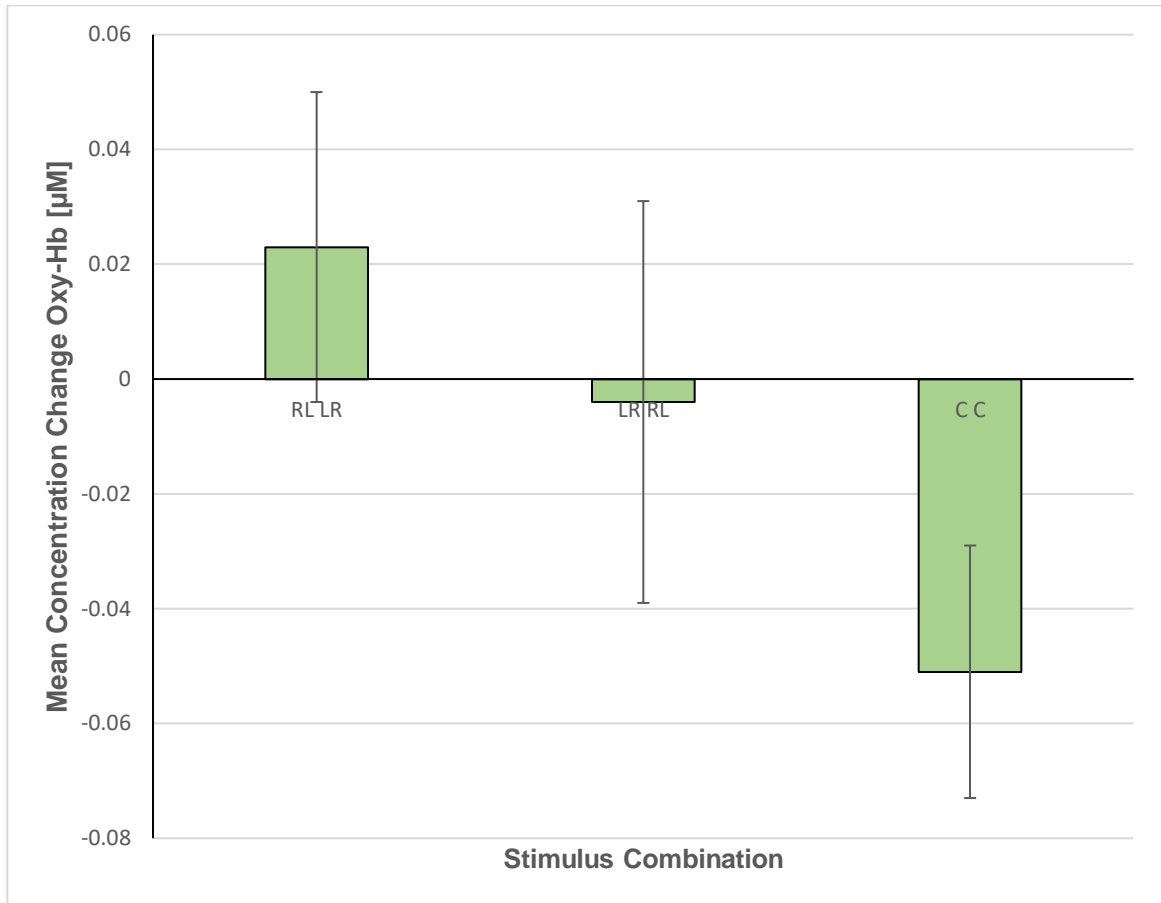
Figure 10: Mean concentration change in oxy-Hb across the 13s-stimulus period in response to the visual presentation of the RL LR, LR RL and C C stimulus sets. All data were averaged across all participants and standard error values are reported.

This comparison was further probed to determine if the LR RL condition "washed out" a potential effect between C C and RL LR. As such, a 2x6 repeated measures ANOVA was run with the independent factors of object (CC and RL LR) and channel (4, 5, 6, 14, 15, 16). A significant main effect for object was revealed ($F_{1,21}= 4.62, p=.043, \eta_P^2 = .54$). Specifically, the increase in oxy-Hb in the right and left hemisphere was significantly greater in response to two relatively optimally graspable objects (M= 0.023 µM) compared to two non-graspable objects (M = -0.051 µM) (Figure 11).
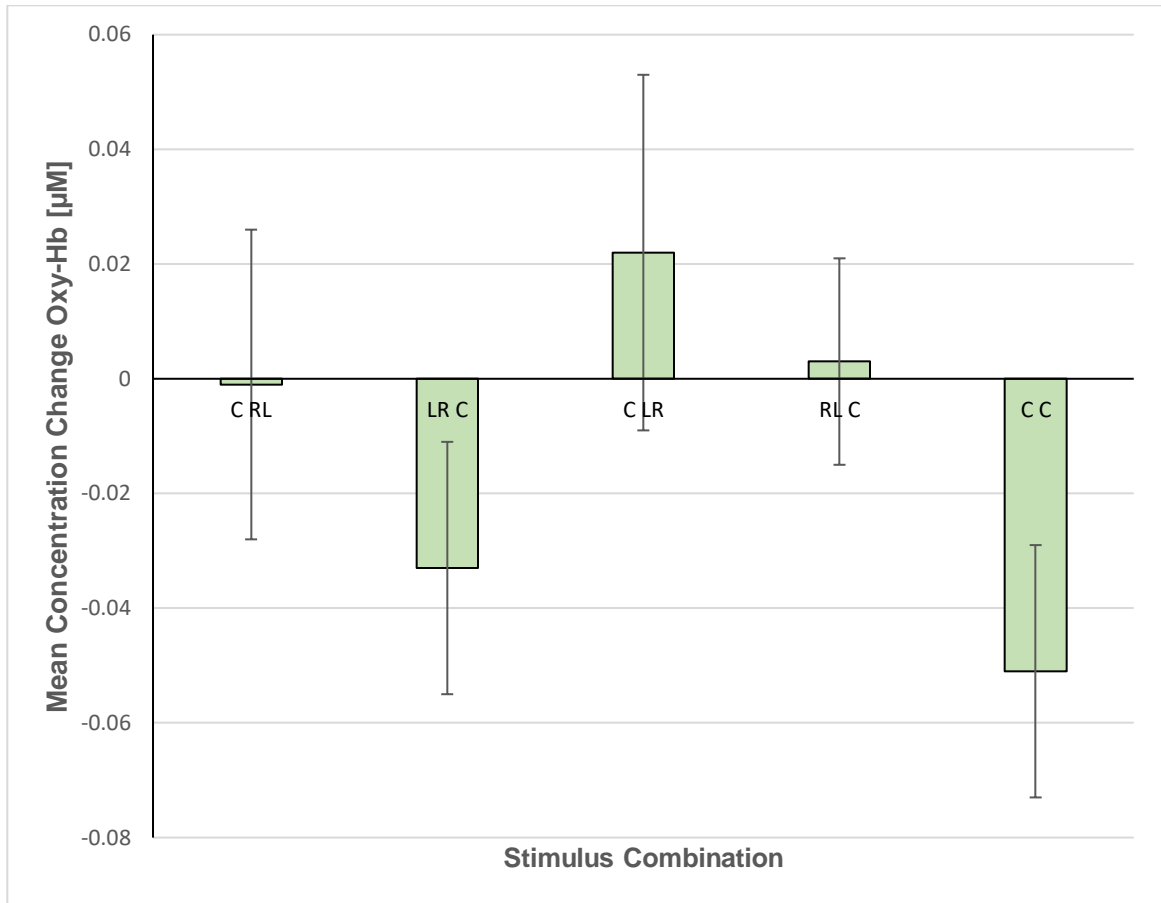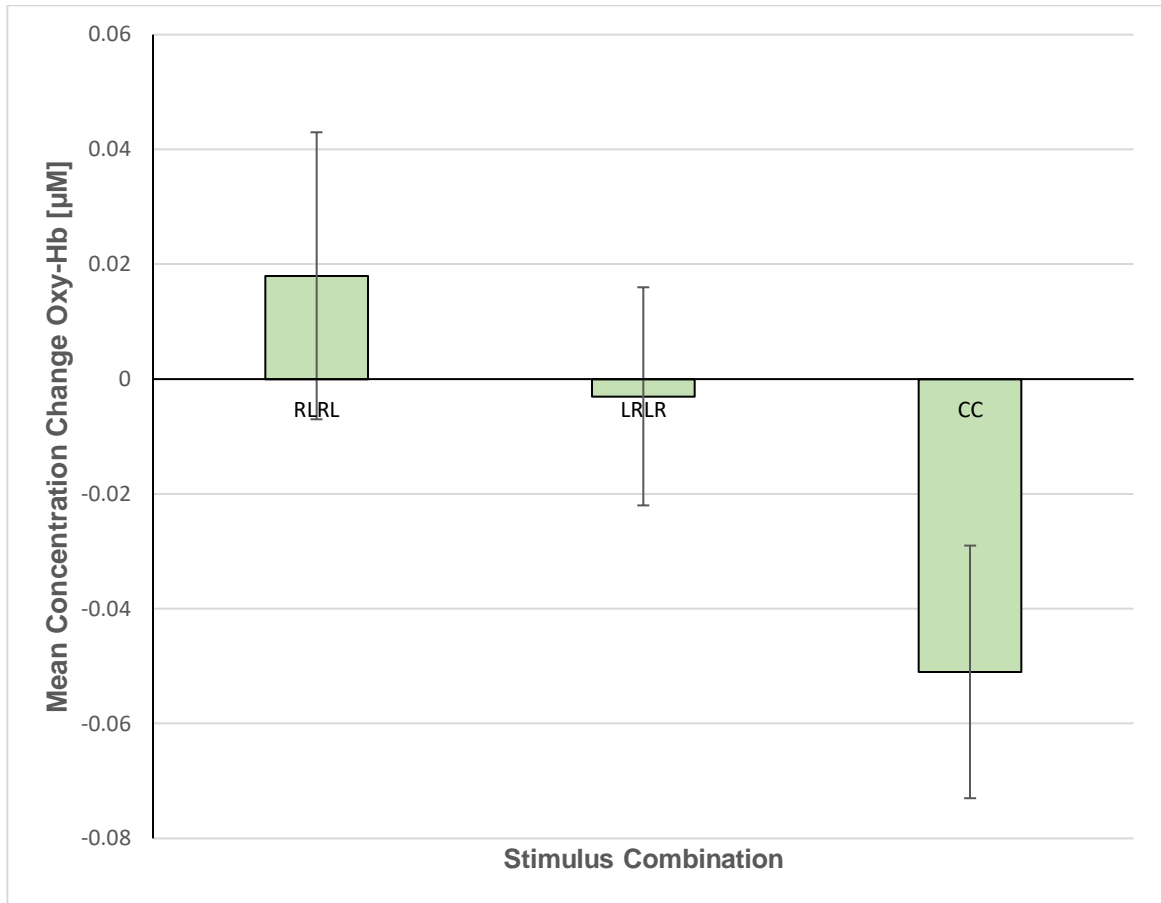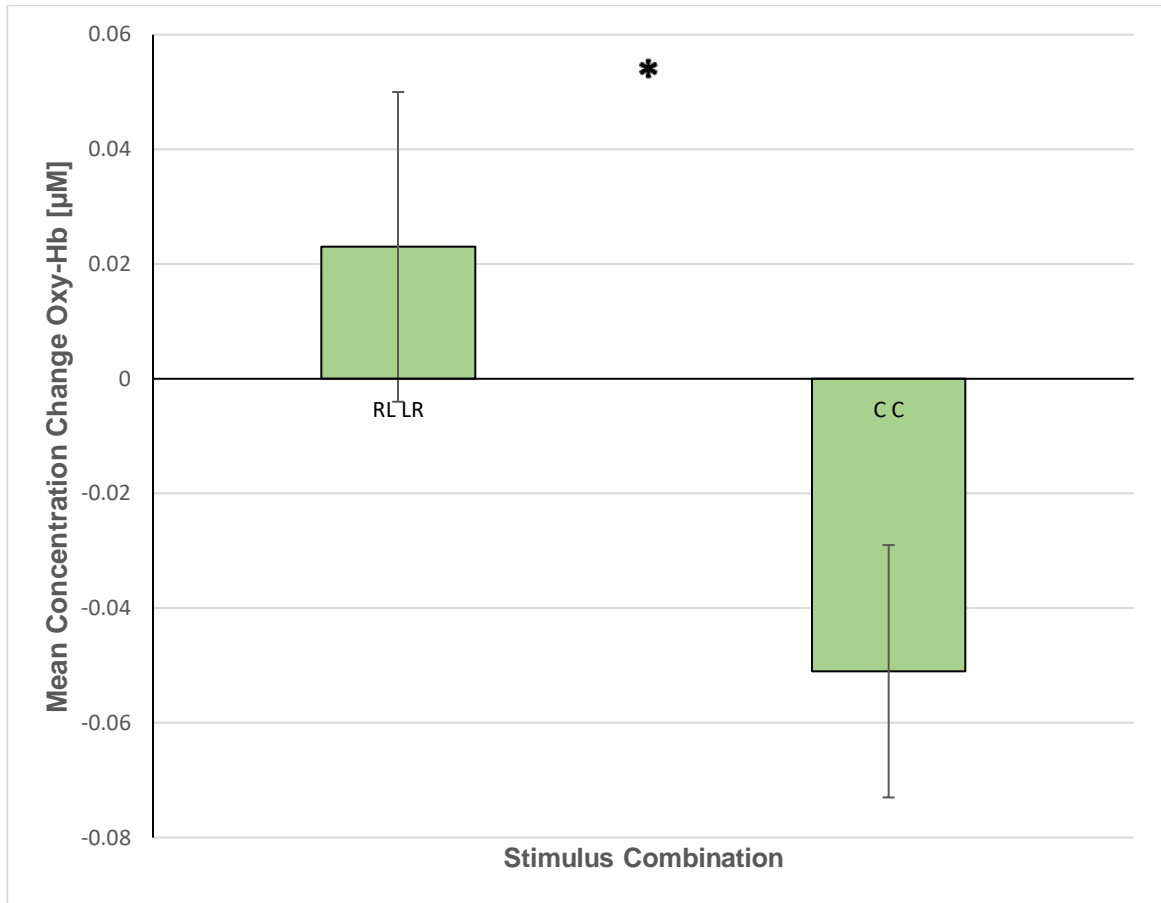
Figure 11: Mean concentration change in oxy-Hb across the 13s-stimulus period in response to the RL LR, and C C stimulus sets. All data were averaged across all participants and standard error values are reported. *Significant difference at $p < 0.05$.

5.0 DISCUSSION

This study sought to examine the effects of object affordances on the perceptual motor system in situations of postural threat. This was performed through three levels of hypothesis testing. First, does the human motor system use visual information to prime actions in the event of a sudden loss of balance? Specifically, is motor action priming driven by the presentation of object visual features (PPA's) that illustrate the potential for the object to be grasped? Second, is fNIRS imaging sensitive enough, as a technique, to detect

neural activation in premotor cortical regions that would suggest priming as a result of the visual presentation of these objects. Third, if priming occurs, to what degree does it reflect the optimality of the object to be utilized in a potential situation of balance threat? Secondary to our main hypotheses was the behavioral data from the study, which aimed to probe the temporal contribution of visional information perceived prior to or during perturbation onset with respect to the success and response choice of perturbation evoked reach to grasp actions.

5.1 Sensing geometry

Due to a paucity of existing literature employing fNIRS to study the contributions of premotor cortices in the planning of reach to grasp actions, evidence for this current experiment was primarily derived from cell recordings performed in primates. Through these findings, it was determined that the premotor cortex was of particular importance in the planning and execution of reach to grasp actions. As a result, a sensing geometry was used to measure hemodynamic changes associated with potential action priming in these regions. As such, the anterior 6 channels of the fNIRS prop were positioned over these premotor and sensorimotor regions. Specifically, channels 4/6 and 14/16 were positioned over left and right Brodmann area 6 (BA6) respectively, while channels 5 and 15 were positioned over the left and right primary somatosensory cortex (S1). The functional roles of these areas are imperative in generating preparatory process that drive and regulate reaching and grasping actions (Sakata et al. 1995; Baumann et al. 2009; Fattori et al. 2010; Fattori et al. 2012; Murata et al. 1997; Raos et al. 2006; Fluet et al. 2010; Bonini et al. 2014a; Vargas-Irwin et al. 2015; Raos et al. 2004).

5.1.2 Brodmann Area 6

BA6, positioned anterior to M1, serves to bridge the pre-frontal and primary motor cortices. Specifically, the caudal region of BA6 has connections to M1, as well as cortical spinal projections, while the rostral region contains connections with the pre-frontal cortex and is absent of a direct connection with the spinal cord. (Barbas & Pandya, 1987; Luppino et al., 1993). BA6 can be further subdivided based on architectonical and functional segregation (Fulton, 1935; Wise, 1985; Freund, 1990). Specifically, this segregation decomposes BA6 into the two major areas, the premotor and supplementary motor cortices (Geyer, et al., 2000).

5.1.3 Premotor Cortex

The lateral portion of BA6, part of the agranular cortex, anterior to the precentral sulcus, contains the premotor cortex (F5) (Stein, 2016). This area projects over the lip of the hemisphere onto the medial portion and contains reciprocal projections with the basal ganglia, cerebellum, posterior parietal, somesthetic and motor cortices. Additionally, this region possesses subcortical projections to the brain stem that act with respect to postural adjustments and locomotion. This region is suggested to control the postural preparation necessary for motor actions (Humphrey, 1979). Specifically, this area is responsible for sensorially guided movements in which the final target position of an arm is planned. This region also has the ability to update this spatial information prior to movement execution as determined through fMRI and rTMS (Benson et al., 1979; Weinric & Wise, 1982; Tanaka, et al., 2005). During intracorticol microstimulation (ICMS), patterns of set related activity suggest that this region acts to reduce the reaction time necessary to produce a

movement, by maintaining a level of activity in corticospinal and rubrospinal cells, in the spinal motor neurons and motor relay neurons, that is nearer to their firing threshold (Weinric & Wise, 1982).

5.1.4 Supplementary Motor Area

The supplementary motor area (SMA) is a medial portion of BA6 that lies rostral to M1 and the paracentral gyri. It is near the convexity of the hemisphere where it projects onto the medial wall (Mihailoff & Haines, 2018). This area receives inputs from the parietal lobe and projects to M1. As such, this region has been suggested to be involved in the planning of muscle activation required to produce a movement (Mihailoff, & Haines, 2018). Through measuring cerebral blood flow with a gamma camera, the SMA has been shown to exhibit a supramotor role, as it is active in relation to complex organized motor tasks (Orgogozao & Larsen, 1979; Roland at al., 1980). Specifically, this region plans complex and simple voluntary movements (Larsson et al., 1996; Grafton et al., 1996; Santosh et al., 1995; Ikeda et al., 1996; Tanji 1984). It has also been suggested that the SMA is active during a preparatory period preceding the initiation of a motor task (Tanji, 1996). Additionally, this region is involved in the temporal structure of a movement, such that motor tasks required to complete the movement are planned with respect to a predetermined ordered (Tanji & Shima, 1994). SMA can be decomposed into the pre-SMA (F6) and SMA proper regions (F3).

5.1.5 Pre-Supplementary Motor Area

The anterior portion of SMA (pre-SMA) is located in the mesial part of BA6 and is evoked through visual information inputs and governs higher-order aspects of motor control. The posterior aspect of SMA is active during simple motor tasks. Specifically, pre-SMA neurons are involved in the preparatory process that regulate upcoming movement. A significantly smaller portion of these neurons are active after movement onset (Mai & Paxinos, 2012).

5.1.6 Supplementary Motor Area Proper

SMA proper has been suggested to possess a supramotor role, as it controls forthcoming movement through the integration of information regarding current limb position and movement goal (Mai & Paxinos, 2012). As such, this region is fundamental in the planning of postures necessary for an upcoming movement (Massion, 1992). Specifically, it is crucial in its role in predictive postural adjustments (Massion, 1992). ICMS studies have reported that this region is involved in integrating preparatory information to create a complete body representation (Luppino et al., 1991).

5.1.7 Primary Somatosensory Cortex

Positioned on the post cenral gyris of the parietal lobe, the primary somatosensory cortex (S1) is the primary receptor of information relating to bodily sensation (Webb, 2017). This information is projected to S1 from skin, muscle, tendons, joints as well as proprioceptive information. S1 consists of four subdivisions, two positioned on the surface of the postcentral gyrus (areas 1 and 2) and two positioned in the posterior bank of the central sulcus (3a and 3b). These regions are all connected to the somatosensory portion of

the thalamus. Specifically, area 3a and 2 are particular importance for the integration of proprioceptive information, as they receive inputs from joint sensors and muscle spindles that measure muscle length (Webb, 2017).

5.2 Common Neural Network

Due to the exploratory nature of this experiment, support for the neurophysiological contributions to affordance motor priming was primarily sought from human and primate studies that employed voluntary reach to grasp action paradigms. These cortical structures may function differently in situations of balance recovery. There is evidence however, to suggest that a common underlying neural mechanism governs the control of both voluntary and perturbation evoked reach-to-grasp actions (Bolton et al., 2011). Although perturbation evoked actions occur approximately 100 ms faster than rapid voluntary actions, similarities in kinematic measures and muscle activity are observed throughout both movements (Gage et al., 2007; Brauer et al. 2002; Maki et al. 2003). Gage et al., (2007) reported deltoid activity onset precedes grip aperture change, which is then followed by wrist movement in both voluntary and perturbation evoked movements. Additionally, peak wrist velocity and peak grip aperture consistently occur at 70% and 94% of the movement time respectively in both actions. Moreover, muscle activity in the triceps coupled with a second burst of muscle activity in the deltoid occurs in order to prepare the arm for anticipation of hand contact by stabilizing the upper limb to provide secure contact between the hand hold and the body. This occurs in both voluntary and perturbation evoked movements (Gage et al., 2007). Additional evidence for this theory was reported by Bolton et al., (2011), who demonstrated that temporary suppression of the hand region of M1, by ways of a cTBS

induced virtual lesion, significantly attenuated response amplitudes during both voluntary and perturbation evoked reach to grasp actions.

5.3 fNIRS Data

Due to the novelty of the current research, the analysis was focused on an *a priori* assumption of where HRF's were likely to be present. By running several *a priori* pairwise comparisons based upon theoretically sound predications of activation loci, we mitigated the risk of influencing the analysis through arbitrary comparisons between unrelated objects. We recognize the subsequent increase in our risk of committing a Type 1 error through this form of analysis; however, this study, to the best of our knowledge, was the first to combine accounts on the influence of objects on the human motor system as posited through ecological psychology and human and primate neurophysiological evidence, with the balance perturbation literature. Additionally, we employed a relatively new method of neural activation detection to measure the potential influence that these objects have on the premotor system. This study, again to the best of our knowledge, was the first to employ this technique to investigate the responses of neural populations present in the premotor cortex to the visual presentation of graspable and non-graspable objects under situations of postural threat. As such, this section discusses the effects that potentially may underlie the data obtained in this study.

Although statistically significant results were not observed across the three levels of comparison, notable tendencies, suggestive of potential effects, did emerge. These tendencies were apparent through visual inspection of the data, but did not produce statistically significant results likely due to the large degree of between-subject variability

present. fNIRS is a relatively new modality for brain imaging that lacks the years of more robust techniques such as fMRI. As such, there are issues inherent with the system, the procedure of the experiment, as well as the data processing that can give rise to issues in the accuracy of the data. Given these limitations, however, the technique has been demonstrated to be robust enough to allow for a general interpretation of the collected data.

5.3.1 Control Condition

Primate studies have reported that when two reaching opportunities are available and no instruction as to which object to grasp is provided, the motor system represents both options concurrently through generating two directionally tuned signals (Cisek & Kalaska, 2005). If one object is nearer to the primates preferred direction of grasp, directionally tuned cells in the dorsal premotor cortex (PMd) discharge (Cisek & Kalaska, 2005). These neuronal populations can be used to reliably predict the subjective response choice of the monkey. This supports a planning model of action wherein multiple grasping opportunities were represented in these premotor populations that were subsequently eliminated based on competition for which target will be reached toward. This occured as more information regarding the object choice was accumulated (Cisek & Kalaska, 2005). These directional signals were sustained until a cue was given with regard to what object to grasp. Following this cue, the directional signal representative of the target that would be grasped, increased, while the signal corresponding to the rejected object decreased. If that stimulus cue represented a different object then was originally preferred by the animal, activity in PMd was updated to reflect this new motor plan, within 100 ms post signal onset and prior to movement initiation (Pastor-Bernier, et al., 2012). This updating activity in PMd also

occured when the monkey freely chose to change its mind regarding what object to grasp. For example, if an option for movement that was originally available became unavailable, these updates and corrections occured in the same cells that were responsible for encoding the original action possibility. As such, the activity in PMd was motor related and specific to the potential reach direction that was being planned by the system that can be modulated by cued instruction or subjective desirability (choice) (Dorris & Glimcher, 2004; Pastor-Bernier & Cisek, 2011).

The above findings could account for the relatively large decreases observed in oxy-Hb in response to the Control condition of the current study. Although not statically significant, it is apparent through observation that relatively large decreases in oxy-Hb in responses to the Control condition occurred across all levels of comparison. If neither object represented an opportunity for grasping, preparatory strategies were not generated in these premotor regions. Specifically, through the visual transformation of the object properties into the potential for action, the system recognized that the object did not afford a grasping opportunity and as such, directionally tuned signals in PMd were not generated. Additionally, the large decreases in oxy-Hb was indicative of substrate being shuttled out of the premotor region to be distributed to other cortical centers. These findings were in line with an affordance-based account of stimulus-response compatibility. Specifically, these accounts hold that differential compatibility effects were created as a function of potential interaction with a given stimulus. These compatibility effects imply an inherent action-system wherein the physical attributes of an object (PPA's) set up the possibility for potential action toward that object (Vingerhoets, et al., 2009). Action was then mediated

primarily based upon potential interaction with a given object, rather than by sensory stimulation caused by the presentation. Attention, however, was not completely excluded and rather may still permit the system to process stimuli relevant to the task and as a result, generate codes directed towards an affordance effect (Vainio et al., 2007; Riggio et al., 2008). In the Control condition, PPA's perceived by the sensorimotor system, would illustrate that the object was not suitable for a grasping action, based on its size, shape and structure. As such, the system did not attend to this information and subsequently did not generate any response priming for an action towards it. These findings are further supported through the behavioral results from part 1 of the experiment in this thesis, that demonstrates no action selection towards these objects in either the right or left hand. In part 2 of this experiment however, it was noted that participants still made attempts toward grasping in the Control condition. Specifically, two attempts were made with the left hand and 13 with the right hand across all participants. When responses made to a Control object were collapsed across all conditions, it was found that two and three responses were made with the left and right hand during part 1 and five and 36 responses from part 2. This accounted for 0.5 and 0.8% of all trials in part 1 and 3.5 and 25% of all trials in part 2 respectively.

These responses during part 2 could have been necessitated by a lack of visual information prior to the fall. As such, the system executed actions that were less accurate and reported responses were a result of errors in the systems evaluation of the objects within that short latency. Secondly, it could represent a genuine attempt by the system to regain balance by grasping the object. In part 1 of the experiment, participants were instructed that the Control condition object represented no grasping opportunity however, in part 2, this

instruction was not provided. It was rather assumed that the instruction carried over from part 1. As such, participants may have assumed that the Control condition could be used as a "last-ditch" effort to mitigate their fall during this part of the experiment. This account would not be likely based on affordance driven motor action priming combined with the observed HRF's reported in part 1 of the experiment. It is likely that these responses were therefore a result of error in the system's ability to generate action when visual information was only given at the onset of instability.

5.3.2 C C - RL LR

No significant results were revealed from the third pairwise comparison. Based on a visual inspection of the data, a subsequent analysis between the Control condition and RL Orthogonal LR Orthogonal condition was performed. Although this comparison was not defined in the original *a priori* set levels of analysis, the level of variability that was present in the data warranted a further estimate of cortical effects at a lower level then what was originally performed during the RL Orthogonal LR Orthogonal condition, LR Orthogonal RL Orthogonal condition, and Control condition analysis.

A statically significant main effect for object was revealed wherein oxy-Hb was greater in response to the RL Orthogonal LR Orthogonal condition compared to the Control condition. This finding suggests that motor action priming of the system occurred when it was presented with two objects that were optimal for a left and right hand grasp. This result is in line with an affordance-based account of stimulus-response compatibility in that affordances differ in their ability to attract attention and thereby influence action. Environmental affordances have been shown to manifest themselves in the speed with

which a response is executed. Tucker and Ellis (1998) suggested that information about "action-relevant" object properties (such as grip type, object orientation, etc.) are represented automatically, or afforded, during the perception of an object and that these properties facilitate object identification (as evidenced by shorter reaction time latencies). As such, visual information including PPA's perceived from the RL Orthogonal LR Orthogonal condition illustrated that both objects afforded an optimal grasping opportunity for the left and right hand, respectively. The cortical processes underlying this motor priming are outlined below.

In response to a perturbation, cortical activity reflects the planning of motor activity that would act to counteract the destabilization from the perturbation (Massion, 1992). Additionally, when an impending perturbation is known, the CNS is set in a state of preparation (central set) that will be required to execute a perturbation evoked compensatory action (Jacobs & Horak, 2007). Central set is a modification to a neuromotor state that occurs due to changes in environmental context (Prochazka, 1989). Within the heightened level of preparation, the system generates action plans towards objects that could be used to mitigate a potential perturbation.

Primate studies have reported that F6 neuronal populations contribute to the encoding of target objects and the grip types that would be used to interact with them. As such, F6 is considered an additional node with F5 for the control of object grasping. F6 exhibits short bursts of phasic activity that peak relatively early whereas F5 exhibits more sustained activity that is tuned based on hand object interaction. These differences in activity illustrate the functional difference of these two population sets. Whereas

visuomotor neurons of F5 allow for visual integration of object features, purely motor neurons of F6 are involved in the encoding of grip types that can be used for action (Lanzilotto, et al., 2016). Additionally, F5 shows preferential activity related to grip types that are natural behavior where as F6 is responsible for the processing of practiced acquired types of action (Macfarlane & Graziano, 2009). Potentially, the grip types used for a left response to an RL Orthogonal object and a right response to an LR Orthogonal object generated the greatest level of neural activity in the detected regions, based on a preference for the motor system to generate responses to the most efficient object choice.

As stated earlier, the visual presentation of two graspable object choices elicited the generation of directional tuned signals that represent both objects. Over time, neural activity representative of the non-preferred grasping object was attenuated, while activity for the preferred option increased until the movement was initiated. It is suggested here that both objects in the RL Orthogonal LR Orthogonal conditions were preferred for the left and right hand, respectively. The potential increase in oxy-Hb could therefore, be indicative of directional signals encoding both objects representations by neuronal populations in F5 and F6 that are priming the system in response for action. This account could also explain the lack of findings in the LR Orthogonal RL Orthogonal condition. Although both objects were graspable, preferential signals would not have been generated towards either object, due to the incompatible nature for both the left and right hand, respectively.

A graspable object affords multiple forms of grip opportunity. Typically, the most optimal form of grasp is selected based on the contextual situation or the goal that is being enacted. During perturbation-evoked actions, the systems goal was to mitigate the fall and

avoid potential damage to the body. This required the generation of rapid targeted action. As such, if the situation permits, using an optimal form to grasp an object (based on the orientation of the object) is paramount in increasing the likelihood of successfully grasping the object, thus maintaining balance. Of all the stimulus combinations presented to participants, the RL Orthogonal LR Orthogonal condition was the most optimal and, by extension, the most likely for the system to execute successful reach-to-grasp actions towards. This explains the relatively large increase in oxy-Hb.

Although oxy-Hb was found to increase in the Control LR Orthogonal, RL Orthogonal Control, and RL Orthogonal RL Orthogonal conditions, this was not great enough to elicit a result that satisfied the threshold of statistical significance when compared to the control. Under the current theory, this could be explained by the directional codes generated for each object. All three stimulus sets were similar in that they only presented one object that was optimal for grasping, be it with the left or right hand. As such, directionally-tuned signals would only be generated for that one object and would subsequently produce lower levels of neural activation relative to the RL Orthogonal LR Orthogonal condition. Additionally, a relative decrease in oxy-Hb was observed in response to the LR Orthogonal Control, Control RL Orthogonal, and LR Orthogonal LR Orthogonal conditions. In the LR Orthogonal Control and Control RL Orthogonal stimulus sets, only one graspable object was presented, however, that object was not optimal for grasping and thus directional signals were not generated. This does not, however, explain the lack of findings observed for the LR Orthogonal LR Orthogonal condition, as one object in the set was optimal for grasping. The most likely account for the negative result in oxy-Hb for this

condition, was due to error in the detected signal determined through visual inspection and numerical calculation of oxy-Hb from the computed HRF's.

5.4 Behavioral Responses (Part 1 & Part 2)

Two cortical behaviors, separated by their temporal relationship to a balance perturbation, govern compensatory balance reactions (Ghafouri et al., 2004; Cheng et al., 2012). These include the visual spatial map that was generated prior to the perturbation, as well as online multisensory information received once the perturbation has been initiated. Due to their temporal differences, separate information is perceived with regard to both processes. The visual spatial map was thus created based on information perceived through exploratory gaze behavior (King et al., 2009; 2010; 2011) whereas online control was specific to information regarding the resulting perturbation (e.g., magnitude, direction and velocity). This relation was probed through the behavioral analysis of the current experiment. Specifically, was visual information received at perturbation onset sufficient to drive successful balance corrective actions? In part 1, visual information was available for a 15 ±5s period prior to perturbation. Conversely, in part 2, visual information was only given at the moment of perturbation onset.

The behavioral results of this experiment suggest that, during perturbation evoked actions, the system was successful in its ability to mitigate a postural perturbation even when vision was only available at the moment of perturbation onset. This suggests that, without prior visual inputs, the system was generating movements of the upper limb based on the context of the perturbation and visual information available after perturbation onset. When a spatial map was generated prior to a perturbation, differential grasp apertures have

been observed to occur based on the direction of chair tilt within 100 ms of wrist movement onset (Gage, et al., 2007). It is suggested that information regarding the kinematics of body motion from vestibular and somatosensory inputs is integrated in cortical regions including the temporal-parietal cortex, supplementary motor area, and prefrontal cortex (De Waele et al., 2001; Ghafouri et al., 2004). This information is considered in conjunction with a visual spatial map related to actions that can be made to counteract the perturbation (De Waele et al., 2001). The results from this experiment suggest that, even at these relatively quick latencies and in the absence of a preformed visual spatial map, the system was still able to drive targeted compensatory actions based exclusively on information received once the perturbation had been initiated. The success of these actions may be attributed to an increase in preparatory cortical activity that supplements the lack of a visual spatial map.

When an impending perturbation was known, the characteristics of the compensatory responses were modified in order to reflect the task condition. These modifications manifest in changes to postural set, which is a state of readiness of the CNS prior to instability and corresponds to the expected task condition (Horak et al., 1989). When the magnitude of the perturbation was unknown, however, the CNS seems to adopt a default set of readiness for a worst-case scenario. The CNS thus engages resources to prepare for the highest level of threat (Mochizuki et al., 2010). This state of preparedness is evidenced by increases in electrodermal response (EDR) amplitudes, which have been reported with increased complexity of a movement required to regain balance (Sibley et al., 2010). As EDR's reflect changes in autonomic sympathetic arousal that are integrated with emotional and cognitive state, these findings reflect the nature of arousal of the system in

response to perturbations (Hugo, 2002). As such, heightened levels of arousal occured prior to perturbation onset when the system recognizes an increase in complexity of the grasping action. This is analogous to a readiness plan or central set of the system where resources are allocated for potential instability (Prochazka, 1989). Due to the lack of visual information prior to the perturbation in the current experiment, it is suggested that the system increased levels of arousal, as well as cortical activity, in order to compensate for the lack of visual spatial map.

Although the post hoc analysis revealed a significant difference between right hand responses to right hand compatible options compared to left hand responses to left hand compatible options, it should still be noted that a greater proportion of hand responses were made to incompatible objects in part 2. Specifically, there was a 10% increase in right responses toward left compatible objects and a 5% increases in left responses toward right compatible objects relative to the experiment comprising part 1 of this study. These findings demonstrate that, although still successful in mitigating the perturbation, these responses are not as optimal as when visual information was available prior to the fall. This is consistent with Cheng et al. (2012), who reported the individual contribution of each temporal event to perturbation evoked reaching and grasping actions. They found that both the stored spatial map and online control provided the system with an adequate amount of information such that successful perturbation evoked reaches could occur despite having only one form of information available. This was observed even for reaches to small handholds that varied unpredictability in location prior to perturbation onset. The reach initiation and arm movements, however, were slowed when depending on only one source

of information. Nevertheless, when both sources of information were available, the system was able to optimally perform the reach to grasp action in the absence of any movement delay.

5.5 Sources of Variability Present in the fNIRS Data

The formation of the fNIRS data is dependent upon, a position, time, and wavelength of the source optode, a medium for which photons can propagate through and experience spectral remittance, as well as detection when exiting the scalp. Variability and noise can, however, be introduced in the fNIRS signal at these levels. In addition, signal contamination can arise from the design of the experimental protocol, motion artifacts, physiological noise such as respiration, cardiac pulsation, blood pressure, as well as biological tissue confounds (Boas, et al., 2004). Although the fNIRS signal reflects the hemodynamic changes in the grey matter, there are confounds in the layer of the head such as the skin and skull, as well as in scalp (blood supply) that can affect the signal data (Gagnon et al., 2012). The results of this experiment illustrate the amount of variability that can be present in the fNIRS signal. This variability can contaminate data and conceal potentially significant results. As such, it is important to understand the origin of these levels of variation, their impact on the fNIRS data and how they can be mitigated in future experiments.

5.5.1 Motion Artifact Correction

fNIRS is less susceptible to MA's compared to other neuroimaging modalities (Lloyd-Fox et al., 2010). There may, however, still be certain head movements that could causes shifts between the source detector pairs and the scalp. These artifacts could manifest

as a shift in the fNIRS baseline signal, suggesting that the correlation between oxy-Hb and deoxy-Hb is more positive than it is (Cooper et al., 2012; Robertson et al., 2010).

MA shifts usually result in a very rapid and large change in magnitude (several orders of magnitude larger) when compared to the tissue-related hemodynamic changes (Tak & Chul Ye, 2014). As a result, qualitative visual inspection is usually performed to identify these large errors (Huppert et al., 2009). Additionally, mathematically based filtering methods are also employed. Although studies have reviewed differences in MA correction techniques, no current standard filtering method currently exists in the literature. As such, variability in the fNIRS signal can arise depending upon the MA correction tool chosen for the experiment. This section will review common methods that are currently employed and how the data is modified with each.

5.5.1.1 Studentized Filter

Studentized filter is a method of outlier detection that is based on the number of standardized deviations between the mean signal and the residual error of a single measurement. The studentized residual is defined by the equation $(y - \hat{y})/\sigma$, where y is the measurement, $\hat{y}$ is the model, and σ is the unbiased estimate of root-mean-squared error of the measurements. This method uses objective criteria to identify and reject data based on a level of standard deviation that defines a rejecting point (i.e., 3 standard deviations). Once these data points are identified, the stimulus block is removed for that temporal region of data.

5.5.1.2 Spline Interpolation

Spline interpolation identifies MA's for each channel using the *hmrMotionArtifactByChannel* function in Homer2 (see section 3.8.1). Once a channel has been determined to possess a MA, the period of data is modeled using a cubic spline function (Scholkmann et al., 2010). The interpolated segment is subtracted from the original and shifted by a value equal to the mean of the segment and the mean of the preceding segment (Yücel et al., 2014). This causes overfitting when trying to replace the MA segment and can ultimately lead to a loss in information (Scholkmann et al., 2010).

5.5.1.3 Wavelet Filtering

This method decomposes the time course containing the data and the MA into a wavelet domain with a discrete wavelet transformation (Molavi et al., 2012). This method operates under the assumption that the wavelet coefficient has a Gaussian probability distribution in which the physiological components of the data are centered around zero and MA's appear as outliers. Parameters set within the wavelet function are used to create a threshold for what determines a MA and once the MA is identified and removed, the function is reconstructed. This method, however, does not correct signal offset and the outlier parameter can often vary between studies. Additionally, this threshold varies depending on if the population is adults or infants (i.e., typically a lower threshold is used for infants). Additionally, this method is poor at removing low-frequency artifacts. MA's that cause a shift in optical density are not corrected and thus, have the potential to negatively impact HRF analysis (Yücel et al., 2014) however, this approach does allow for

a good localization of the abrupt and rapid signal changes caused by the MA's (Molavi & Dumont, 2012; Sato et al., 2006).

5.5.1.4 Principal Component Analysis (PCA)

A PCA creates a matrix of measurements in which the data are arranged as a number of time point by a number of channels. This matrix is then transformed into a set of orthogonal vectors in decreasing order based on the amount of variance present in each. The main assumption that underlies this process is that a MA, if to occur, would be equally present in all channels. This MA would also possess a similar temporal variation among these channels and, as such, the variation can be inferred to be a result of the MA. As such, the PCA is set to remove a certain number of components based on the percent variance observed across all channels. Typically, this involves one component being removed or 80% of the variance. The signal is then reconstructed with the remaining components. This analysis, however, is not specific to a temporal region and rather is applied to transform the entire time series of all the data for all channels. This presents problems as functional signals not impacted by MA's may be removed, which has been shown to occur specifically in activation signals in adult participants (Zhang, et al., 2005).

5.5.1.5 Targeted Principal Component Analysis (tPCA)

In contrast, a tPCA uses the same procedure as described above, but only transforms a period of data that is defined to possess a MA. This sequence is defined in the processing stream of Homer2 using the *hmrMotionArtifact-ByChannel* function. Once the segment of time possessing the MA is identified, the components are ranked in decreasing order of variance. A N_{tPCA} number of components are then projected out of the data to account for

97% of the variance. The epochs of corrected motion are then brought back together. This technique has been shown to overcome the issue of over correcting data that contains the functional signal (Zhang et al., 2005). Additionally, tPCA is more robust in recovering hemodynamic response functions from MA impacted data when compared to both wavelet based filtering and spline interpolation. Specifically, tPCA produces a significant reduction in mean-squared error and enhancement in Pearson's correlation coefficient to the actual HRF (Yücel et al., 2014). For this reason, the tPCA was used in this experiment.

5.5.2 Skin Blood Flow Removal

Interference in the fNIRS signal can arise from the superficial layers of the scalp (Gagnon, et al., 2011). This includes blood in the skin of the head, as well as interference that can occur with other biological tissue in the area. A PCA, in combination with a short separation channel, can be used to decompose the signal based off of assumptions of orthogonality and statistical reduction of noise (Tak & Chul Ye, 2014). Through PCA, it is assumed that the baseline signal will contain this interference and that it remains constant over time. This baseline signal is recorded from a short separation channel, that has a detector optode spacing less the 30 mm. This causes the specificity of the detection of photons to be representative of those that passed through the scalp and not into the skull. As a result, hemodynamic concertation can be inferred to be a product of blood in the scalp tissue. Therefore, by projecting fNIRS data onto this baseline signal, a reduction of skin blood flow noise can be achieved. It has been shown that using this method can produce more localized fNIRS responses with an increase in the contrast-to-noise ratio when compared to other filtering methods (Zhang et al., 2005). The fNIRS system used in this

experiment did not have a short separation channel. Correction to the best of our ability was performed by baseline correcting stimulus data to a time period prior to each trial. As cortical hemodynamic changes are expected to be relatively low during baseline, any increases could theoretically arise from the scalp and skull. This method does not consider hemodynamic increases in the scalp during the stimulus protocol. As such, variability and noise could have been introduced into the signal due to these tissues confounds.

5.5.3 Systematic Noise

Systematic noise can arise from respiration, cardiac pulsation, blood pressure and Mayer waves. In order to remove these factors of noise from the fNIRS signal, bandpass filtering can be employed. Specifically, a low-pass filter can be used to remove high frequency noise produced by cardiac pulsations, typically at 1 Hz (60 × beats/min). A high pass filter can be used to remove slow, low frequency noise produced by blood pressure oscillations, typically found between 0.08-0.12 Hz (Huppert et al., 2009). The bandpass filter used in this experiment was set with a high pass filter at .02 Hz and a low pass filter at .5 Hz. Variation can be introduced into the fNIRS signal based on the specific bandpass filter frequencies chosen (Kaiser et al., 2014; Yücel et al., 2014; Hofmann et al., 2008). Careful consideration must be taken when choosing the appropriate low and high pass filter cut offs as to not remove frequencies associated with the hemodynamic response.

Although bandpass filters can be used to remove low and high frequency noise, there may be frequencies of noise associated with the functional hemodynamic signal. These are usually respiratory components of the blood pressure signal that overlap with the hemodynamic data. As a result, a filtering method in which each source is defined in space

and time is required (Boas et al., 2004). Baseline correction can be used, in which the spatiotemporal covariance of the baseline data is used to filter systemic variations present in the brain activation signal. This illustrates the importance of collecting a baseline signal prior to each experimental trial, as these systematic noises can change throughout the experimental procedure, specifically if physical exertion is required. As such, each trial data is corrected based on the baseline measure recorded prior to that trial.

5.5.4 Individual Anatomical Variation

Partial optical path length is used in fNIRS as an indicator of the sensitivity of the signal to absorption changes in the brain. This is accomplished by approximation of the derivative of the changes in optical density as light passes through the tissue versus the absorption coefficient of the brain tissue (Nakamura et al., 2016). This cannot be accomplished through experimentation and rather is calculated based on head models and numerical analysis of light propagation (Okada et al., 1996).

The sensitivity of the fNIRS signal that traverses the volume of grey matter is dependent on several anatomical factors. These factors introduce between participant variability that may manifest as part of the data. Typical penetration depth of NIR-light is 2 to 3 cm with a source detector distance set at 3 cm. From the source optode on the head, the light travels through the scalp (0.5-1 cm), skull (0.5-1 cm) and cerebral spinal fluid (CSP) (0-2 mm) layers. These layers encompass the distance the light travels from the scalp to the cortex (SCD) and impacts the penetration and scattering of the light (Huppert et al., 2009; Custo et al., 2006). These layers have been shown to vary depending on age, gender or other inter-participant factors (Huppert et al., 2009; Custo et al., 2006). Specifically,

penetration depth of NIR-light has been shown to be inversely proportional to SCD (Haeussinger, et al., 2011). This impacts the amount of light that reaches the grey matter and is absorbed (Heinzel et al., 2013, Cui et al., 2011). As such, the sensitivity of grey matter detection (GMD) decreases with increases in SCD. Therefore, GMD maybe small in some participants that possess a lager SCD. Additionally, the thickness of these layers varies across the head, thereby impacting channels differently depending on which region of the head they are positioned (Kawaguchi et al., 2007, Haeussinger et al., 2011).

The individual tissue characteristics that compose the SCD have differing impacts on the penetration depth of the NIR-light. Specifically, the majority of GMD reduction with increases in SCD, is attributed to the skull and scalp, however, the CSF layer attenuates the reduction of GMD, due to the low scattering properties of the fluid (Haeussinger et al., 2011). These differences in thickness affect the partial optical path length of the light photons (Nakamura et al., 2016). In addition, the brain has been shown to expand or otherwise move within the skull to a limited degree causing changes in the thickness of the CSF layer (Firbank et al., 1998). As the SCD becomes larger, so too does the thickness of the CSF layer. The thickness of the skull layer however, predominately causes the reduction in GMD (Okada & Delpy, 2003). Nevertheless, an over proportional CSF layer thickness may attenuate the reduction in GMD, in a participant with a large skull layer. Therefore, it is not the mere SCD that impacts GMD, but rather the specific partial path lengths experienced by specific tissue types that need to be considered when estimating the sensitivity of GMD. Additionally, grayification of the cortex has the potential to affect GMD sensitivity in extreme cases of sulcal geometry.

These tissue factors have been calculated using Monte Carlo simulations in which photon migration in a highly scattering biological tissue can be modeled with different head and tissue parameters (Van der Zee & Delpy, 1987; Fukui et al., 2003; Okada & Delpy, 2003; Boas et al., 2002). This variability can therefore, be accounted for by incorporating anatomical volumetric data from magnetic resonance imaging (MRI) for each participant. By doing so, the spatial characteristics of the skull and scalp that the light will travel through can be accounted for, thus improving the user's knowledge of the GMD for each participant. Specifically, an individual segmentation of the skin, skull, CSF, white and grey matter layers could to be conducted. This would allow for the digitization of these layers onto a participant's head, in which the sour detector optodes could be co-registered and the partial optical path length calculated (Tremblay et al., 2018).

5.5.5 Variation from Prop Shift During Fall

The factor that could most significantly reduce the quality of the fNIRS spatial resolution, and introduce variation into the signal, is the sensing geometry of the source detector pairs (Herrera-Vega et al., 2017). As a result, it is imperative that the optodes are placed correctly over the scalp. Additionally, the optodes must be as secured as possible to eliminate potential motion artifacts (Huppert et al., 2009). The best way to achieve stability is through pressure between the optode and the scalp, however, the more pressure that is applied, the more uncomfortable it is for the participant. No specific pressure values have been identified in the literature, as it varies by region of the scalp and between participants, in part due to individual differences in head shape. This does illustrate, however, that tight cranial head wear in all scalp areas is required for proper testing (Kassab & Sawan, 2014).

Specifically, general head measurements in accordance with the 10-20-system are taken using 4 skull landmarks (nasion, inion, left pre-ocular point, and right pre-ocular point). These measurements are used to ensure that the cap size properly fits the participants head. Caps that are too large or small can cause differentiation in the spatial resolution of the signal.

In the current study, participants' heads were measured to ensure that the proper cap size was used. In addition, once the cap was placed over the participant's head, hair was carefully removed from each source detector position, to ensure a clear connection between the optode and the participants scalp. Once the hair was carefully removed using a *Q-tip*, the optodes were fixed into position using spring tension caps that added pressure to the optodes to maintain placement of the optodes over the scalp. An additional cap was placed over the optodes and tightened with zippers to further increases the pressure on the probes and prevent movement. All wires from the optodes were carefully fixed to the rear of the chair to prevent tension on the optodes under the cap (see section 3.7.2.) Despite these precautions, it is still possible that the optodes shifted during the posterior perturbation. The perturbation was a large whole body instability that triggered a rapid compensatory action. The force and magnitude of these movements may have caused the cap to lift off the head and move slightly under the cap. This could have introduced inter-individual variability between the expected cortical detection area and the location of the true measurement. In addition, due to the anatomical differences discussed above, shifts in the cap could position the optodes in areas where the layers of the SCD differed from the original position (Kawaguchi et al., 2007, Haeussinger et al., 2011).

5.5.6 Instrumental Noise

Instrumental noise can be introduced into the fNIRS signal from the computer, hardware, or from noise in the surrounding space (Huppert et al., 2009). This noise typically poses a uniform frequency spectrum. fNIRS sampling frequency occurs at a higher rate than the hemodynamic changes being measured. The majority of signal power at the higher sampled frequencies is therefore, dominated by instrumental noise. As such, the majority of the high frequency instrument noise can be removed from the physiological data by means of a low-pass filter. Additionally, certain tests and calibration can be performed with the system to better attenuate the instrumental noise, thus reducing variability the may be present in the data.

fNIRS systems can be adjusted in terms of their detector gain and intensity of emitted light, to better control for the influence of external noise (Huppert et al., 2009). For the system used in the current study, this occurs during the calibration period prior to data acquisition. Additionally, optodes must be shielded from ambient light by covering them with opaque materials to mitigate the impact of stray light on the detection of NIR-light. In the current experiment, a heavy black cap was placed over the optodes. In order to mitigate instrumental noise, a dark noise test is performed prior to data acquisition. This test evaluated the optical sensitivity of each detector to ensure proper functioning of the hardware. If a dark noise test is not performed, there may be damage to the hardware that can negatively affect the detectors sensitivity and introduce a large amount of instrument noise into the signal.

5.5.7 Variation in Cortical Region Measurement

The registration of functional data to common brain space allowed for the projection of hemodynamic changes onto cortical surfaces measured by the sensing geometry of a study. Currently, the MNI coordinate system is the gold standard and most common stereotaxic platform for achieving this (Brett et al., 2002). The MNI template was created through the registration of multiple subject averages from MRI's to the Talairach brain (Collin et al., 1994). A major problem exists, however, in the ability for research to validate MNI mapping data across participants when no structural images (MRI) for each participant is available. MRI data acquisition is expensive and sometimes outside the means of a research lab for a particular study. In order to reduce between-subject and within-subject variability in these types of experiments, the location of each optode should be mapped onto the head surface of a participant using the 10-20 system. The variability in cortical mapping is influenced by the distance between the optode and the reference point that is used for placing the optode on the head (Okamoto & Dan, 2005; Singh et al. 2005). Previous studies have found a close correlation between MNI coordinates determined from MRI and 10-20 system reference locations with a standard deviation of 4.7 to 7.0 mm for optodes positioned over the prefrontal region (Singh et al., 2005). Not all fNIRS prop designs, however, allow for specific placement of each optode over each predetermined 10-20 reference location. This is commonly due the fNIRS cap. Although the cap can stretch over the participant's head, it is impossible to individually adjust each optode position without interfering with a neighboring optode. Typically, as was the case in the current

study, one or two optodes were positioned over a 10-20 reference point and the other optodes were assumed to be positioned over the other reference points for that specific sensing geometry. For example, in the current study, C3 and C4 were used as reference points for detectors 3 and 7 respectively. The reliability of this technique, however, was tested in this experiment.

Specifically, NIRSite was used to determine the positions of the optodes over each 10-20 reference point. These were cross checked by digitizing the x, y, and z coordinates of each optode on an actual human head using neuronavigation. The standard deviation of each optode position for each system was calculated. Specifically, coordinates x and z illustrated large levels of variation between the two systems. This illustrates the difference between what is expected through the 10-20 reference system and what is actually achieved from a participant's head. If the MNI coordinates had been based off of the 10-20 reference points, there would be a large discrepancy between the cortical surfaces identified and what was actually being measured.

As such, we accounted for this variation to the best of our ability, by registering the digitized coordinates to a Collin atlas. This atlas was then used to determine the corresponding detecting channels in MNI space. Using this single atlas as a reference, the cortical structures being measured by the sensing geometry of this study was inferred to remain constant across all participants, in order to allow for multi-subject analysis. Nevertheless, this technique can introduce inter-individual variability as it is assumed the cap stretch is proportional across all participants and that the optodes are in a similar position over the head.

5.6 Conclusion

Perturbation-evoked reach to grasp actions are driven by a complex neural network among specific frontal and parietal circuits that allow for the most efficient arm and hand movement to successfully grasp an object (e.g., Jeannerod et al., 1995). These actions involve cortical networks consisting mainly of the parietal, premotor and primary motor cortices (e.g., Rizzolatti & Luppino, 2001). The current experiment, to the best of our knowledge, was the first of its kind in examining hemodynamic changes in the pre-motor cortices in response to the visual presentation of objects, in situations of balance threat. This was assessed through the fNIRS brain imaging. We recognize, however, that participants may have not perceived the posterior perturbation as an actual threat, due to the features that were implemented to ensure participant safety. It may be that these evolutionary derived behaviors of rapid compensatory action are only elicited when a true threat of damage to the system is detected. In order to account for this, the apparatus in the current experiment was built to replicate the one used by Gage et al., (2007) by delivering a similar form of perturbation (i.e., seated in a chair) at a similar acceleration (i.e., between 1-2 m/s^2). Under these parameters, Gage et al., showed that muscle activity onset and movement kinematics were representative of a rapid compensatory action to a threatening balance perturbation. Although muscle activity onset was not measured in the current experiment, we suggest that the actions aimed at reestablishing balance were initiated in a similar temporal window and followed similar movement kinematics.

Although the conclusions that can be drawn from the current experiment are

somewhat limited, these findings do serve as a first step in understanding the cortical impact object affordances have on the perceptual motor system and how they might affect motor priming for perturbation-evoked recovery actions. Specifically, the behavioral results of this experiment suggest that the system is complex enough in its organization and execution of perturbation evoked actions, that the lack of a visual spatial map does not prevent the system from successfully mitigating balance perturbations. Online multisensory feedback, integrated with visual inputs received at the moment of perturbation onset, are sufficient in driving successful perturbation evoked actions. In addition, the cortical measures suggest that object affordances have the potential to prime motor actions in the premotor and sensorimotor cortices, when both objects are optimal for grasping. These findings also suggest the potential for fNIRS to be sensitive enough in detecting premotor priming, at least at this level of activation.

Additionally, this study sought to outline the potential problems that face fNIRS data collection and processing, and their subsequent impact on the interpretation of results. Through a better awareness of the sources of variation and noise that contaminate the signal, as well as methods that can deal with these effects, a more optimal way of employing these methodologies for studying premotor priming was suggested. In conclusion, this study offers the first insight into the exploration of the cortical effect of object affordances beyond their use in volitional reach to grasp actions. It is through a better understanding of the innate mechanism that drive and regulate postural balance, that will increase our understanding of how the sensorimotor system and our actions, are influenced by physical features of objects in our environment.

6.0 REFERENCES

Ackermann H, Dichgans J, Guschlbauer B. (1991). Influence of an acoustic preparatory signal on postural reflexes of the distal leg muscles in humans. *Neurosci Lett*. 127:242–246.

ADA standards for accessible deisgn (2010). Department of justice

Akiyama, T., Ohira, T., Kawase, T., Kato, T. (2006). TMS orientation for NIRS functional motor mapping. *Brain Topogr*. 19: 1–9.

Akram, S., Miyasike-daSilva, V., Ooteghem, K., McIlroy, W. (2013). Role of peripheral vision in rapid perturbation-evoked reach-to-grasp reactions. *Exp. Brain Res*. 229: 609–619.

Attwell, D., Laughlin SB. (2001). An energy budget for signaling in the grey matter of the brain. *J Cereb Blood Flow Metab*21:1133–1145.

Barbas, H., Pandya, D. (1987). Architecture and frontal cortical connections of the premotor cortex (area 6) in the rhesus monkey. *J Comp Neurol*. 256:211–228.

Baumann, M., Fluet, M., Scherberger, H. (2009). Context-specific grasp movement representation in the macaque anterior intraparietal area. *J Neurosci*. 29(20):6436 6448.

Benson, D., Hienz, D., Goldstein, H. (1979). Observations on unit activity in monkey auditory cortex and dorsolateral frontal cortex during a sound localization task. *Sot. Neurosci.Abstr*. 5: 16.

Boas, D., Chen, K., Grebert, D., Franceschini, M. (2004). Improving the diffuse optical imaging spatial resolution of the cerebral hemodynamic response to brain activation in humans. *Opt Lett*. 29:1506–1508.

Boas, D., Culver, J., Stott, J., Dunn, A. (2002). Three dimensional monte carlo code for photon migration through complex heterogeneous media including the adult human head. *Opt Express*. 10: 159–70.

Boas, D.A., Dale, A.M., Franceschini, M.A. (2004). Diffuse optical imaging of brain activation: approaches to optimizing image sensitivity, resolution, and accuracy. *Neuroimage* 23 (Suppl. 1), S275–S288.

Boden, S., Obrig, H., Kohncke, C., Benav, H., Koch, S.P., Steinbrink, J. (2007). The oxygenation response to functional stimulation: is there a physiological meaning

to the   lag between parameters? *Neuroimage* 36, 100–107.

Bolton, DAE., Patel, R., Staines, WR., McIlroy, WE. (2011). Transient inhibition of primary motor cortex suppresses hand muscle responses during a reactive reach to grasp. *Neuroscience Letter*. 504, no. 2 (n.d.): 83–87.

Bonini, L., Maranesi, M., Livi, A., Fogassi, L., Rizzolatti, G. (2014a). Space-dependent representation of objects and other's action in monkey ventral premotor grasping neurons. *J Neurosci.* 34(11):4108–4119.

Borra, E., Belmalih, A., Calzavara, R., Gerbella, M., Murata, A., Rozzi, S., (2008). Cortical connections of the macaque anterior intraparietal (AIP)   area. *Cereb. Cortex* 18, 1094 1111. doi: 10.1093/cercor/bhm146.

Brauer, S., Woollacott, M., Shumway-Cook, A. (2002). The influence of a concurrent cognitive task on the compensatory stepping response to a perturbation in balance impaired and   healthy elders. *Gait Posture*. 15:83–93.

Brett, M., Johnsrude, I., Owen, A. (2002). The problem of functional localization in the human brain. *Nature Rev Neurosci*. 3:243–249.

Buccino, G., Sato, M., Cattaneo, L., Roda, F., & Riggio, L. (2009). Broken affordances, broken objects: a TMS study. *Neuropsychologia*. 47, 3074–3078.

Burleigh A, Horak F. (1996). Influence of instruction, prediction, and afferent sensory information on the postural organization of step initiation. *J Neurophysiol*. 75:16191628. [PubMed: 8727400]

Cardellicchio, P., Sinigaglia, C., Costantini, M. (2011). The space of affordances: a TMS study. *Neuropsychologia.* 49, no. 5 (n.d.): 1369–72.

Chan, CW., Jones, GM., Kearney, RE., Watt, DG. (1979). The 'late' electromyographic response to limb displacement in man. I. Evidence for supraspinal contribution. *Electroencephalogr   Clin Neurophysiol*; 46:173– 181. [PubMed: 86424].

Chance, B., Leigh, J. S., Miyake, H., Smith, D. S., Nioka, S., Greenfeld, R. et al. (1988). Comparison of time-resolved and -unresolved measurements of deoxyhemoglobin in brain. *Proceedings of the National Academy of Science USA*, 85(14), 4971 4975.

Chance, B., Zhuang, Z., UnAh, C., Alter, C., & Lipton, L. (1993). Cognition-activated low frequency modulation of light absorption in human brain. *Proceedings of the National Academy of Science USA,* 90(8), 3770–3774.

Cheng, K., McKay, S., King, E., Maki, B. (2012). Reaching to recover balance in unpredictable circumstances: Is online visual control of the reach-to-grasp reaction necessary or sufficient? *Exp Brain Res*. 218:589–599.

Cisek, P. (2001). Embodiment is all in the head. *Behav. Brain Sci. 24*, 36–38.

Cisek, P., Kalaska, J. (2005). Neurol correlates of reaching decision in dorsal premotor cortex: specification of multiple direction choices and final selection of action. *Neuron*. 45: 801814.

Colier, W.N., Quaresima, V., Baratelli, G., Cavallari, P., van der Slujis, M., Ferrari, M. (1997).Detailed evidence of cerebral hemoglobin oxygenation changes in response to motor cortical activation revealed by continuous wave spectrophotometer with 10 Hz temporal resolution. *SPIE.* 2979: 390–396.

Collins, D., Neelin, P., Peters, T., Evans, A. (1994). Automatic 3-D intersubject registration of MR volumetric data in standardized Talairach space. *J. Comput. Assist. Tomogr*. 18 (2), 192–205.

Cooper, R.J., Selb, J., Gagnon, L., Phillip, D., Schytz, H.W., Iversen, H.K., Ashina, M., Boas, D.A. (2012). A systematic comparison of motion artifact correction techniques for functional near-infrared spectroscopy. *Front. Neurosci.* 6.

Cope, M. (1991). The application of near infrared spectroscopy to non invasive monitoring of cerebral oxygenation in the newborn infant. *Department of Medical Physics*.

Cope, M., Delpy, D. (1988). System for long-term measurement of cerebral blood and tissue oxygenation on newborn infants by near infra-red transillumination. *Medical and Biological Engineering and Computing* 26, no. 3 289–94.

Crevecoeur, F., Thonnard, JL., Lefevre, P., Scott, SH. (2016). Long-latency feedback coordinates upper-limb and hand muscles during object manipulation tasks. *eNeuro*. http://dx.doi.org/10.1523/eneuro. 012915.2016.

Critchley, H. (2002). Electrodermal responses: what happens in the brain. *The Neuroscientist*. 8, 132–142.

Cui, X., Bray, S., Bryant, D., Glover, G., Reiss, L. (2011). A quantitative comparison of NIRS and fMRI across multiple cognitive tasks. *NeuroImage*. 54, 2808–2821.

Custo, A., Wells, W., Barnett, A., Hillman, E., Boas, A. (2006). Effective scattering coefficient of the cerebral spinal fluid in adult head models for diffuse optical imaging. *Appl Opt*. 45:4747–4755.

Davare M., Andres M., Cosnard G., Thonnard J.L., Olivier E. (2006). Dissociating the role of ventral and dorsal premotor cortex in precision grasping. *J. Neurosce.* 26:2260–2268.

Davare M., Duque J., Vandermeeren Y., Thonnard J.L., Olivier E. (2007). Role of the ipsilateral primary motor cortex in controlling the timing of hand muscle recruitment. *Cereb. Cortex.* 17: 353–362.

Davare, M., Kraskov, A., Rothwell, J., Lemon, R. 2011. Interactions between areas of the cortical grasping network. *Curr Opin Neurobiol.* 21(4):565–570.

Davare, M., Rothwell, J., Lemon, R. (2010). Causal connectivity between the human anterior intraparietal area and premotor cortex during grasp. *Current Biology.* 20(2): 176–181.

De Waele, C., Baudonniere, P., Lepecq, J., Tran Ba Huy, P., Vidal, P. (2001). Vestibular projections in the human cortex. *Exp Brain Res.* 141(4): 541–551.

Desai, N., & Valentino, D. J. (2011). A software tool for quality assurance of computed/digital radiography (CR/DR) systems.

Diener, HC., Dichgans, J., Bootz, F., Bacher, M. (1984). Early stabilization of human posture after a sudden disturbance: influence of rate and amplitude of displacement. *Exp Brain Res*; 56:126–134. [PubMed: 6468561]

Dorris, M., Glimcher, P. (2004). Activity in posterior parietal cortex is correlated with the relative subjective desirability of action. *Neuron.* 44:365–378.

Durduran, T., Yu, G., Burnett, M.G., Detre, J.A., Greenberg, J.H., Wang, J., Zhou, C., Yodh, A.G. (2004). Diffuse optical measurement of blood flow, blood oxygenation, and metabolism in a human brain during sensorimotor cortex activation. *Opt. Lett.* 29, 17661768.

Ellis, R., and Tucker, M. (2000). Micro-affordance: the potentiation of components of action by seen objects. *Br. J. Psychol.* 91(pt 4), 451–471. doi: 10.1348/000712600161934.

Fadiga, L., Fogassi, L., Gallese, G. & Rizzolatti, G. (2000). Visuomotor neurons: Ambiguity of the discharge or "motor" perception? *International Journal of Psychophysiology* 35:165   77.

Fattori, P., Breveglieri, R., Bosco, A., Gamberini, M., Galletti, C. (2015). Vision for prehension in the medial parietal cortex. *Cereb* Cortex.

doi:10.1093/cercor/bhv302.

Fattori, P., Breveglieri, R., Raos, V., Bosco, A., Galletti, C. (2012). Vision for action in the macaque medial posterior parietal cortex. *J Neurosci*. 32(9):3221–3234.

Fattori, P., Raos, V., Breveglieri, R., Bosco, A., Marzocchi, N., Galletti, C. (2010). The dorsomedial pathway is not just for reaching: grasping neurons in the medial parieto occipital cortex of the macaque monkey. *J Neurosci*. 30(1):342–349.

Ferrari, Gallese, Rizzolatti, Fogassi (2003). Mirror neurons responding to the observation of ingestive and communicative mouth actions in the monkey ventral premotor cortex. European *Journal of Neuroscience*. 17: 1703-1714.

Firbank, M., Okada, E., & Delpy, D. T. (1998). A theoretical study of the signal contribution ofregions of the adult head to near-infrared spectroscopy studies of visual evoked responses. *Neuroimage*, 8(1), 69–78.

Fluet, M., Baumann, M., Scherberger, H. (2010). Context-specific grasp movement representation in macaque ventral premotor cortex. *J Neurosci*. 30(45):15175 15184.

Fogassi L., Gallese V., Buccino G., Craighero L., Fadiga L., Rizzolatti G. (2001). Cortical mechanism for the visual guidance of hand grasping movements in the monkey: A reversible inactivation study. *Brain*. 124: 571–586.

Foglia, S., Lyons, J. (2019). The effect of object orientation as a function of affordance on motor action priming. *In preparation.*

Fox, P. T., Raichle, M. E., Mintun, M. A., Dence, C. (1988). Nonoxidative glucose consumption during focal physiologic neural activity. *Science*, 241(4864), 462 464.

Franca, M., Turella, L., Canto, R., Brunelli, N., Allione, L., Golfré Andreasi, N., Desantis, M., Marzoli, D., Fadiga, L. (2012). Corticospinal facilitation during observation of graspable objects: a transcranial magnetic stimulation study. *PlosONE.* https://doi.org/10.1371/journal.pone.0049025.

Franceschini, M.A., Fantini, S., Thompson, J.H., Culver, J.P., Boas, D.A. (2003). Hemodynamic evoked response of the sensorimotor cortex measured noninvasively with near-infrared optical imaging. *Psychophysiology* 40, 548–560.

Freund, H. (1990). Premotor area and preparation of movement. Rev Neurol. 146:543 547.

Fukui, Y., Ajichi, Y., Okada, E. (2003). Monte carlo prediction of near-infrared light

propagation in realistic adult and neonatal head models. *Applied optics*. 42: 2881–7.

Fulton, J. (1935). Definition of the "motor" and "premotor" areas. *Brain*. 58: 311–316.

Gage, WH., Zabjek, KF., Hill, SW., McIlroy, WE. (2007). Parallels in control of voluntary and perturbation evoked reach-to-grasp movements: EMG and kinematics. *Exp. Brain Res*. 181: 627–637.

Gagnon, L., Perdue, K., Greve, D., Goldenholz, D., Kaskhedikar, G., Boas, D. (2011). Improved recovery of the hemodynamic response in diffuse optical imaging using short optode separations and state-space modeling. *Neuroimage* 56 (3), 1362 1371.

Gagnon, M.A. Yucel, M. Dehaes, R.J. Cooper, K.L. Perdue, J. Selb, T.J. Huppert, R.D. Hoge, D.A. Boas (2012). Quantification of the cortical contribution to the NIRS signal over the motor cortex using concurrent NIRS-fMRI measurements. *NeuroImage*. 59: 3933–3940.

Gallese V., Murata A., Kaseda M., Niki N., Sakata H. (1994). Deficit of hand preshaping after muscimol injection in monkey parietal cortex. *Neuroreport*. 5: 1525–1529.

Gentilucci, M., Fogassi, L., Luppino, G., Matelli, M., Camarda, R. & Rizzolatti, G. (1988). Functional organization of inferior area 6 in the macaque monkey. I. Somatotopy and the control of proximal movements. *Exp. Brain. Res*., 71, 475 490.

Gerbella, M., Belmalih, A., Borra, E., Rozzi, S., and Luppino, G. (2011). Cortical connections of the anterior (F5a) subdivision of the macaque ventral premotor area F5. *Brain Struct. Funct*. 216, 43–65. doi: 10.1007/s00429-010-0293-6.

Geyer, S., Matelli, M., Luppino, G., Zilles, K. (2000). Functional neuroanatomy of the primate isocortical motor system. *Anat Embryol*. (6):443-74.

Ghafouri M, McIlroy WE, Maki BE (2004). Initiation of rapid reach- and-grasp balance reactions: is a pre-formed visuospatial map used in controlling the initial arm trajectory? *Exp Brain Res* 155:532–536

Gibson, A.P., Hebden J.C., Arridge, S.R. (2005) recent advances in diffuse optical imaging. *Phys Med Biol*. 50: 1-43.

Gibson, J. J. (1979). The ecological approach to visual perception. Boston: Houghton Mifflin.

Gold, J.I., and Shadlen, M.N. (2001). Neural computations that underlie decisions about sensory stimuli. *Trends Cogn. Sci. 5*, 10–16.

Goodale, M. A., and Milner, A. D. (1992). Separate visual pathways for perception and action. *Trends Neurosci*. 15, 20–25. doi: 10.1016/0166-2236(92)90344-8.

Gottlieb GL, Agarwal GC. (1980). Response to sudden torques about ankle in man. II. Postmyotatic reactions. *J Neurophysiol.* 43:86–101. [PubMed: 7351552]

Grafton, S. (2010). The cognitive neuroscience of prehension: recent developments. *Exp Brain Res*. 204(4):475–491.

Grafton, S., Fagg, A., Woods, R., Arbib, M. (1996). Functional anatomy of pointing and grasping in humans. *Cereb Cortex.* 6:226-237.

Gratton G, Goodman-Wood MR, Fabiani M (2001). Comparison of neuronal and hemodynamic measures of the brain response to visual stim. *Hum Brain Mapp.* 13: 13-25.

Gratton, E., Toronov, V., Wolf, U., Wolf, M., Webb, A. (2005). A measurement of brain activity by near-infrared light. *J Biomed Opt*. 10:011008.

Gratton, G., Maier, JS., Fabiani, M., Mantulin, WW., Gratton, E. (1994). Feasibility of intracranial near-infrared optical-scanning.   *Psychophysiology.* 31: 211-215

Grin L, Frank J, Allum JH. (2007). The effect of voluntary arm abduction on balance recovery following multidirectional stance perturbations. *Exp Brain Res*. 178:62 78.

Haeussinger, F., Heinzel, S., Hahn, T., Schecklmann, M., Ehlis, A. (2011). Simulation of near infrared light absorption considering individual head and prefrontal cortex anatomy: implications for optical neuroimaging. *PLoS ONE*. 6(10): e26377. doi:10.1371/journal.pone. 0026377.

Hall, CN., Klein-Flügge, MC., Howarth, C., Attwell, D. (2012). Oxidative phosphorylation, not glycolysis, powers presynaptic and postsynaptic mechanisms underlying brain information processing. *JNeurosci.* 26: 8940 8951.

Hayakawa, Nemoto, Iino, Kasai (2005). Rapid Ca^{2+}-dependent increase in oxygen consumption by mitochondria in single mammalian central neurons. *Cell Calcium* 37: 359-370.

Heinzel, S., Haeussinger, F., Hahn, T., Ehlis, A., Plichta, M., Fallgatter, A. (2013). Variability of (functional) hemodynamics as measured with simultaneous fNIRS and fMRI during intertemporal choice. *Neuroimage*. 71:125-134.

Hepp-Reymond, M.C., Huesler, E.J., Maier, M.A. & Qi, H.-X. (1994). Force- related neuronal activity in two regions of the primate ventral premotor cortex. *Can. J. Physiol. Pharmachol.*, 72, 571–579.

Herrera-Vega, J., Treviño-Palacios, C., Orihuela-Espina, F. (2017). Neuroimaging with function near infrared spectroscopy: from formation to interpretation. *Infrared physics & technology* 85: 225-237.

Hirase, H., Creso, J. & Buzsaki, G (2004). Capillary level imaging of local cerebral blood flow in bicuculline-induced epileptic foci. *Neuroscience* 128, 209–216.

Hirth, C., Obrig, H., Valdueza, J., Dirnagl, U., Villringer, A., (1997). Simultaneous assessment of cerebral oxygenation and hemodynamics during a motor task. A combined near infrared and transcranial Doppler sonography study. *Adv. Exp. Med. Biol*. 411, 461–469.

Hofmann, M., Herrmann, M., Dan, I., Obrig, H., Conrad, M., Kuchinke, L., Jacobs, A., Fallgatter, A. (2008). Differential activation of frontal and parietal regions during visual word recognition: An optical topography study. *NeuroImage*. 40, 1340 1349.

Horak, FB., Diener, HC., Nashner, LM. (1989). Influence of central set on human postural responses. *J Neurophysiol* 62:841–853.

Horovitz, S.G., Gore, J.C. (2003). Studies of the sensitivity of near infrared spectroscopy to detect changes in levels of brain activation due to manipulation of motor tasks. *25th Annual Conference of the IEEE EMBS*, Cancun, Mexico.

Hoshi, Y. (2003). Functional near-infrared optical imaging: Utility and limitations in human brain mapping. *Psychophysiology*, 40(4), 511–520.

Hugo, C. (2002). Review: Electrodermal Responses: What Happens in the Brain. *The Neuroscientist*. 8(2):132–142

Humphrey, D. (1979). On the cortical control of visually directed reaching: Contributions by non-precentral motor areas. *Posture and Movement*. 51-112.

Huppert, T., Diamon, A., Franceschini, M. Boas, D. (2009). HomER: a review of time series analysis methods for near-infrared spectroscopy of the brain. *Appl Opt*. 48: 280-298.

Huppert, T.J., Hoge, R.D., Diamond, S.G., Franceschini, M.A., Boas, D.A., (2006). A temporal comparison of BOLD, ASL, and NIRS hemodynamic responses to motor stimuli.

Ikeda, A., Lüders H., Shibasaki, H., Collura, T., Burgess, R., Morris, H., Hamano, T. (1996). Movement-related potentials associated with bilateral simultaneous and unilateral movements recorded from human supplementary motor area. *Electroencephalogr Clin Neurophysio.* 95: 323-334.

Irani, F., Platek, S., Bunce, S., Ruocco, A., Chute, D. (2007). Functional near infrared spectroscopy (fNIRS): an emerging neuroimaging technology with important applications for the study of brain disorders. *The Clinical Neuropsychologist.* 21:9–37.

Izzetoglu, K., Bunce, S. B. O., Pourrezaei, K., & Chance, B. (2004). Functional optical brain imaging using NIR during cognitive tasks. *International Journal of Human– Computer* Interaction, 17, 211–227.

Jacobs JV, Fujiwara K, Tomita H, Furune N, Kunita K, Horak FB (2008). Changes in the activity of the cerebral cortex relate to postural response modification when warned of a perturbation. *Clin Neuro- physiol* 119:1431–1442.

Jacobs, J., Horak, F. (2007). Cortical control of postural responses. *J Neural Transm* 114:13391348.

Jasdzewski, G., Strangman, G., Wagner, J., Kwong, K.K., Poldrack, R.A., Boas, D.A. (2003). Differences in the hemodynamic response to event-related motor and visual paradigms as measured by near-infrared spectroscopy. *Neuroimage* 20, 479–488.

Jeannerod, M., Arbib, M. A., Rizzolatti, G., and Sakata, H. (1995). Grasping objects: the cortical mechanisms of visuomotor transformation. *Trends Neurosci*. 18, 314–320. doi: 10.1016/0166-2236(95)93921-J.

Jensen JL, Brown LA, Woollacott MH (2001). Compensatory stepping: the biomechanics of a preferred response among older adults. *Exp Aging Res* 27:361–376.

Jobsis, F. F. (1977). Non-invasive, infrared monitoring of cerebral and myocardial oxygen sufficiency and circulatory parameters. *Science*, 198(4323), 1264–1267.

Kaas, J., Stepniewska, I. (2016). Evolution of posterior parietal cortex and parietal-frontal networks for specific actions in primates. *J Comp Neurol.* 524(3):595–608.

Kalaska, J. F., Sergio, L. E. & Cisek, P. (1998). Cortical control of whole-arm motor tasks. In: *Sensory guidance of movement, Novartis Foundation SymposiumNo. 218.*

Kassab, A., Sawan, M. (2014). The NIRS cap: key part of emerging wearable brain device interfaces. *IntechOpen*. http://dx.doi.org/10.5772/67457.

Kawaguchi, H., Koyama, T., Okada, E. (2007). Effect of probe arrangement on reproducibility of images by near-infrared topography evaluated by a virtual head phantom. *Applied Optics*. 46: 1658–68.

Kety, S. (1957). The general metabolism of the brain *in vivo. Metabolism of the nervous system*.pp 221–237.

Kim, J.N., and Shadlen, M.N. (1999). Neural correlates of a decision in the dorsolateral prefrontal cortex of the macaque. *Nat. Neurosci. 2*, 176–185.

Kimura, T. et al. (2006). Transcranial magnetic stimulation over sensorimotor cortex disrupts anticipatory reflex gain modulation for skilled action. *J. Neurosci.* 26, 9272–9281.

King, C., McKay, S., Lee, T., Scovil, C., Peters, A., Maki, B. (2009). Gaze behavior of older adults in responding to unexpected loss of balance while walking in an unfamiliar environment: a pilot study. *J Optom* 2:119–126.

King, E., Lee, T., McKay, S., Scovil, C., Peters, A., Pratt, J., Maki, B. (2011). Does the ''eyes lead the hand'' principle apply to reach-to-grasp movements evoked by unexpected balance perturbations? *Hum Mov Sci.* 30:368–383.

King, E., McKay, S., Cheng, K., Maki, B. (2010). The use of peripheral vision to guide perturbation-evoked reach-to-grasp balance-recovery reactions. *Exp Brain Res.* 207:105 118.

Krutky, M.A. et al. (2013). Influence of environmental stability on the regulation of end point impedance during the maintenance of arm posture. *J. Neurophysiol.* 109, 1045–1054.

Kurata, K. & Tanji, J. (1986). Premotor cortex neurons in macaques: activity before distal and proximal forelimb movements. *J. Neurosci.*, 6, 403–411.

Kurtzer, I. et al. (2009). Long-latency responses during reaching account for the mechanical interaction between the shoulder and elbow joints. *J. Neurophysiol.* 102, 3004–3015.

Kurtzer, I. et al. (2010). Long-latency and voluntary responses to an arm displacement can be rapidly attenuated by perturbation offset. *J. Neurophysiol*. 103, 3195–3204.

Kurtzer, I.L. (2014). Long-latency reflexes account for limb bio- mechanics through several supraspinal pathways. *Front. Integr. Neurosci*. 8, 99.

Kurtzer, I.L. et al. (2008). Long-latency reflexes of the human arm reflect an internal model of limb dynamics. *Curr. Biol.* 18, 449–453.

Lanzilotto, M., Livi, A., Maranesi, M., Gerbella, M., Barz, F., Ruther, P., Fogassi, L., Rizzolatti, G., Bonini, L. (2016). Extending the cortical grasping network: pre supplementary motor neuron activity during vision and grasping of objects. *Cerebral Cortex*. 26: 4435–4449.

Larsson, J., Gulyas, B., Roland, P. (1996). Cortical representation of self- paced finger movement. *Neuroreport.* 7:463-468.

Leff, D., Orihuela-Espina, F., Elwell, CE., Athanasiou, T., Delpy, DT., Darzi, AW., Yang, GZ. (2011). Assessment of the cerebral cortex during motor task behaviours in adults: a systematic review of functional near Infrared spectroscopy (fNIRS) studies. *NeuroImage*. 54, no. 4 (n.d.): 2922–36.

Lloyd-Fox, S., Blasi, A., Elwell, C. (2010). Illuminating the developing brain: the past, present and future of functional near infrared spectroscopy. *Neurosci. Biobehav. Rev.* 34 (3), 269–284.

Lu, M., Preston, J., Strick, P. (1994). Interconnections between the prefrontal cortex and the premotor areas in the frontal lobe. *J Comp Neurol.* 341:375–392.

Luppino, G., Matelli, M., Camarda, R., Gallese, V., Rizzolatti, G. (1991). Multiple representations of body movements in mesial area 6 and the adjacent cingulate cortex: An intracortical microstimulation study. J. Comp. Neurol. 311:463482.

Luppino, G., Matelli, M., Camarda, R., Rizzolatti, G. (1993). Corticocortical connections of area F3 (SMA-proper) and area F6 (pre-SMA) in the macaque monkey. *J Comp Neurol.* 338:114 –140.

Luppino, G., Murata, A., Govoni, P., Matelli, M. (1999). Largely segregated parietofrontal connections linking rostral intraparietal cortex (areas AIP and VIP) and the ventral premotor cortex (areas F5 and F4). *Exp. Brain Res*. 128, 181–187. doi: 10.1007/s002210050833.

Macfarlane, B., & Graziano, M. S. (2009). Diversity of grip in Macaca mulatta. *Exp. Brain Res*. 197, 255–268. doi: 10.1007/s00221-009-1909-z.

Mackert, B.M., Leistner, S., Sander, T., Liebert, A., Wabnitz, H., Burghoff, M., Trahms, L., Macdonald, R., Curio, G. (2008). Dynamics of cortical neurovascular coupling analyzed by simultaneous DC-magnetoencephalography and time-resolved near infrared spectroscopy. *Neuroimage* 39, 979–986.

Mai, J., Paxinos, G. (2012). The human nervous system (3rd Edition). Elsevier. ISBN: 9780080921303

Maki, B., McIlroy, W. (1997). The role of limb movements in maintaining upright stance: the "change-in-support" strategy. *PhysTher* 77:488–507.

Maki, B., McIlroy W., Fernie, G. (2003). Change-in-support reactions for balance recovery. *IEEE Eng Med Biol* Mag. 22:20–26.

Maki, B., Whitelaw, S. (1993). Influence of expectation and arousal on center-of-pressure responses to transient postural perturbations. *J Vestib Res.* 3:25–39.

Maki, A., Yamashita, Y., Ito, Y., Watanabe, E., Mayanagi, Y., Koizumi, H. (1995). Spatial and temporal analysis of human motor activity using noninvasive NIR topography. *Med. Phys.* 22, 1997–2005.

Maki, A., Yamashita, Y., Watanabe, E., Koizumi, H. (1996). Visualizing human motor activityby using non-invasive optical topography. *Front. Med. Biol. Eng.* 7, 285 297.

Makris, S., Hadar, K., Yarrow, K. (2011). Viewing objects and planning actions: on the potentiation of grasping behaviours by visual objects. *Brain and Cognition* 77, no. 2: 257–64.

Maranesi, M., Bonini, L., Fogassi, L. (2014). Cortical processing of object affordances for self and others' action. *Front Psychol.* 5:538.

Marr, D. (1982). Vision: a computational investigation into the human representation and processing of visual information, Henry Holt and co. New York, NY.

Marteniuk, R. G. (1976). Information processing in motor skills. New York: Holt, Rinehart and Winston.

Massion, J. (1992). Movement, posture and equilibrium: Interaction and coordination. *Progress in Neurobiology.* 38: 35-56.

Matelli, M., Luppino, G., Rizzolatti, G. (1991). Architecture of superior and mesial area 6 and the adjacent cingulate cortex in the macaque monkey. *J Comp Neurol*. 311(4):445–462.

McDannald, D. W. (2018) Motor Affordance for Grasping a Safety Handle. *Neuroscience Letter*. 683, 131–37.

McIlroy, W., Maki, B. (1993). Changes in early 'automatic' postural responses associated with the prior-planning and execution of a compensatory step. *Brain Res*. 631:203–211.

Mehagnoul-Schipper, D.J., van der Kallen, B.F., Colier, W.N., van der Sluijs, M.C., van Erning,L.J., Thijssen, H.O., Oeseburg, B., Hoefnagels, W.H., Jansen, R.W., Mapp (2002).Simultaneous measurements of cerebral oxygenation changes during brain activation by near-infrared spectroscopy and functional magnetic resonance imaging in healthy young and elderly subjects. *Hum. Brain Mapp*. 16, 14–23.

Michaels, C. F. & Carello, C. (1981). Direct Perception. Englewood Cliffs, NJ: Prentice Hall. Miyai, I., Tanabe, H.C., Sase, I., Eda, H., Oda, I., Konishi, I., Tsunazawa, Y., Suzuki, T., Yanagida, T., Kubota, K. (2001). Cortical mapping of gait in humans: a near-infrared spectroscopic topography study. *Neuroimage* 14, 1186 1192.

Mihailoff, G., Haines, D. (2018). *Fundamental neuroscience for basic and clinical applications* (fifth edition). (Elsevier, Philedelphia).

Milgram, P. (1987). A spectacle-mounted liquid-crystal tachistoscope. *Behavior Research Methods*. 19(5):449-456.

Miyai, I., Tanabe, H., Sase, I., Eda, H., Oda, I., Konishi, I., Tsunazawa, Y., Suzuki, T., Yanagida, T., Kubota, K. (2001). Cortical mapping of gait in humans: a near infrared spectroscopic topography study. *NeuroImage*. 14:1186–1192.

Mochizuki, G. (2010). Perturbation-evoked cortical activity reflects both the context and consequence of postural instability. *Neuroscience*. 2: 599–609.

Molavi, B., Dumont, G.A. (2012). Wavelet-based motion artifact removal for functional near infrared spectroscopy. *Physiol. Meas*. 33 (2), 259–270.

Muhogora, W., Bonutti, F., Kazema, R., Padovani, R., & Msaki, P. (2011). Performance evaluation of three computed radiography systems using methods recommended

in American Association of Physicists in Medicine Report 93. *Journal of Medical Physics, 36*(3), 138-146.

Murata A., Fadiga L., Fogassi L., Gallese V., Raos V., Rizzolatti G. (1997). Object representation in the ventral premotor cortex (area F5) of the monkey. *J. Neurophysiol.* 78: 2226–2230.

Murata, A., Gallese, V., Luppino, G., Kaseda, M., and Sakata, H. (2000). Selectivity for the shape, size, and orientation of objects for grasping in neurons of monkey parietal area AIP. *J. Neurophysiol.* 83, 2580–2601.

Nakamura, K., Kurihara, K., Kawaguchi, H., Obata, T., Ito, H., Okada, E. (2016). Estimation of partial optical path length in the brain in subject specific head models for near-infrared spectroscopy. *Optical Review* 23, no. 2: 316–22.

Obrig, H. & Villringer, A. (2003). Beyond the visible—imaging the human brain with light. *Journal of Cerebral Blood Flow and Metabolism*, 23(1), 1–18.

Obrig, H., Hirth, C., Junge-Hulsing, J.G., Doge, C., Wenzel, R., Wolf, T., Dirnagl, U., Villringer, A. (1997). Length of resting period between stimulation cycles modulates hemodynamic response to a motor stimulus. *Adv. Exp. Med. Biol.* 411, 471–480.

Obrig, H., Hirth, C., Junge-Hulsing, J.G., Doge, C., Wolf, T., Dirnagl, U., Villringer, A. (1996a). Cerebral oxygenation changes in response to motor stimulation. *J. Appl. Physiol.* 81, 1174–1183.

Okada, E., Delpy, D. (2003). Near-infrared light propagation in an adult head model. II. Effect of superficial tissue thickness on the sensitivity of the near-infrared spectroscopy signal. *Appl. Opt.* 42, 2915.

Okada, E., Delpy, D. (2003). Near-infrared light propagation in an adult head model. i. modeling of low-level scattering in the cerebrospinal fluid layer. *Applied optics*. 42: 2906–14.

Okada, E., Schweiger, M., Arridge, S.R., Firbank, M., Delpy, D.T(1996). Experimental validation of Monte Carlo and finite-element methods for the estimation of the optical path length in inhomogeneous tissue. *Appl. Opt.* 35, 3362.

Okamoto, M., Dan, I. (2005). Automated cortical projection of head-surface locations for transcranial functional brain mapping. *NeuroImage*. 26, 18–28.

Oldfield, RC. (1971) The assessment and analysis of handedness: the Edinburgh inventory, *Neuropsychologia*. 9: 97–113.

Orgogozo, J., Larsen, B. (1979). Activation of the supplementary motor area during voluntary movements in man suggests it works as a supramotor area. *Science*. 206:847-850.

Pastor-Bernier, A., Cisek, P. (2011). Neural Correlates of Biased Competition in Premotor Cortex. *The Journal of Neuroscience*. 31(19):7083–7088.

Pastor-Bernier, A., Tremblay, E., Cisek, P. (2012). Dorsal premotor cortex is involved in switching motor plans. *Frontiers in Neuroengineering*. Doi: 10.3389/fneng.2012.00005.

Plichta, M.M., Herrmann, M.J., Ehlis, A.C., Baehne, C.G., Richter, M.M., Fallgatter, A.J. (2006). Event-related visual versus blocked motor task: detection of specific corticalactivation patterns with functional near-infrared spectroscopy. *Neuropsychobiology* 53, 77–82.

Posner, M. (1982). Cumulative development of attentional theory. *American Psychologist*, 37, 168-179.

Prochazka, A. (1989). Sensorimotor gain control: a basic strategy of motor systems *Prog. Neurobiol*. 33, 281–307.

Proverbio, M. A., Adorni, R., & D'Aniello, G. E. (2011). 250 ms to code for action affordance during observation of manipulable objects. *Neuropsychologia*. 49, 2711–2719.

Pruszynski, J.A. Scott, S.H. (2012). Optimal feedback control and the long-latency stretch response. *Exp. Brain Res*. 218, 341–359

Raos V., Umiltá M., Murata A., Fogassi L., Gallese V. (2006). Functional properties of grasping-related neurons in the ventral premotor area F5 of the macaque monkey. *J. Neurophysiol*. 95: 709–729.

Raos, V., Umiltá, M., Gallese, V., Fogassi, L. (2004). Functional properties of grasping related neurons in the dorsal premotor area F2 of the macaque monkey. *J Neurophysiol*. 92(4): 1990–2002.

Raos, V., Umiltá, M., Murata, A., Fogassi, L., Gallese, V. (2006). Functional properties of grasping-related neurons in the ventral premotor area F5 of the macaque monkey. *J Neurophysiol*. 95(2):709–729.

Rice N.J., Tunik E., Grafton S.T. (2006). The anterior intraparietal sulcus mediates grasp execution, independent of requirement to update: New insights from transcranial magnetic stimulation. J. *Neurosci*. 26:8176–8182.

Riggio L., Iani C., Gherri E., Benatti F., Rubichi S., Nicoletti R. (2008). The role of attention in the occurrence of the affordance effect. *Acta Psychol*. 127: 449–458.

Rizzolatti, G., and Fadiga, L. (1998). Grasping objects and grasping action meanings: the dual role of monkey rostroventral premotor cortex (area F5). *Novartis Found Symp*. 218, 81 95; discussion 95–103.

Rizzolatti, G., Camarda, R., Fogassi, L., Gentilucci, M., Luppino, G., and Matelli, M. (1988). Functional organization of inferior area 6 in the macaque monkey. II. Area F5 and the control of distal movements. *Exp. Brain Res*. 71, 491–507. doi: 10.1007/BF00248742.

Rizzolatti, G., Luppino, G. (2001). The cortical motor system. *Neuron*. 31(6):889-901.

Rizzolatti, G., and Matelli, M. (2003). Two different streams form the dorsal visual system: anatomy and functions. *Exp. Brain Res.* 153, 146–157. doi: 10.1007/s00221-003-1588-0.

Robertson, F.., Douglas, T., Meintjes, E. (2010). Motion artifact removal for functional near infrared spectroscopy: a comparison of methods. *IEEE Trans. Biomed. Eng*. 57 (6),1377–1387.

Roland, P., Larsen, B., Lassen, N., Skinhej, E. (1980). Supplementary motor area and other cortical areas in organization of voluntary movements in man. *J Neurophysiol.* 43:118 136.

Rossignol, S. et al. (2006). Dynamic sensorimotor interactions in locomotion. *Physiol. Rev*. 86, 89–154.

Rozzi, S., Coude, G. (2015) Grasping actions and social interaction: neural bases and anatomical circuitry in the monkey. *Front. Psychol*. 6:973.

Sakata, H., Taira, M., Murata, A., and Mine, S. (1995). Neural mechanisms of visual guidance of hand action in the parietal cortex of the monkey. *Cereb. Cortex* 5, 429–438. doi: 10.1093/cercor/5.5.429.

Sander, T.H., Liebert, A., Burghoff, M., Wabnitz, H., Macdonald, R., Trahms, L. (2007a. Cross correlation analysis of the correspondence between magnetoencephalographic and near infrared cortical signals. *Meth. Inf. Med*. 46, 164–168.

Sarraf, T., Marigold, D., Robinovitch, S. (2014). Maintaining standing balance by handrail grasping. *Gait & Posture*. 39, 258-264.

Sato, H., Kiguchi, M., Maki, A., Fuchino, Y., Obata, A., Yoro, T., Koizumi, H. (2006). Within subject reproducibility of near-infrared spectroscopy signals in sensorimotor activation after 6 months. *J. Biomed*. Opt. 11, 014021.

Santosh, C., Rimmington, J., Best, J. (1995). Functional magnetic resonance imaging at 1 T: motor cortex, supplementary motor area and visual cortex activation. *Br J Radiol.* 68: 369-374.

Scholkmann, F., Spichtig, S., Muehlemann, T., Wolf, M. (2010). How to detect and reduce movement artifacts in near-infrared imaging using moving standard deviation and spline interpolation. *Physiol Meas*. 31(5): 649–662.

Schroeter, M., Bucheler, M., Muller, K., Uludag, K., Obrig, H., Lohmann, G., Tittgemeyer, M., Villringer, A., Von Cramon, D. (2004). Towards a standard analysis for functional near infrared imaging. *NeuroImage*. 21:283–290.

Schroeter, M., Kupka, T., Mildner, T., Uludag, K., Von Cramon, D. Y. (2006). Investigating the post-stimulus undershoot of the BOLD signal: A simultaneous fMRI and fNIRS study. *Neuroimage*, 30, 349–358.

Scott, SH. (2016). A functional taxonomy of bottom-up sensory feedback processing for motor actions. *Trends in Neuroscience.* Vol. 39, No. 8.

Scott, SH., Cluff, T., Lowrey, C., Takei, T. (2015). Feedback control during voluntary motor actions. *Curr.Opin.* Neurobiol. 33, 85–94.

Shemmell, J., An, JH., Perreault, EJ. (2009). The differential role of motor cortex in stretch reflex modulation induced by changes in environmental mechanics and verbal instruction. *J. Neurosci*. 29, 13255–13263.

Shumway-Cook, A., Woolacott, M. (1995). Motor control: theory and practical applications. Williams & Wilkins, Baltimore.

Singh. A., Okamoto, M., Dan, H., Jurcak, V., Dan, I. (2005). Spatial registration of multichannel multi-subject fNIRS data to MNI space without MRI. *Neuroimage*. 27(4):842-51.

Sibley, K., Lakhani, B., Mochizuki, G., McIlroy, W. (2010). Perturbation-evoked electrodermal responses are sensitive to stimulus and context-dependent manipulations of task challenge. *Neuroscience Letters*. 485: 217-221.

Soechting, J.F., Lacquaniti, F. (1988). Quantitative evaluation of the electromyographic

responses to multidirectional load perturbations of the human arm. *J. Neurophysiol*. 59, 1296-1313.

Sokoloff L (1960). The metabolism of the central nervous system *in vivo*. *Handbook of Physiology, Section I, Neurophysiology*. 3: 1843–1864.

Stein, J. (2016). *Reference module in neuroscience and biobehavioral psychology*. (Elsevier)

Strangman, G., Culver, J.P., Thompson, J.H., Boas, D.A. (2002). A quantitative comparison of simultaneous BOLD fMRI and NIRS recordings during functional brain activation. *Neuroimage* 17, 719–731.

Strangman, G., Franceschini, M.A., Boas, D.A. (2003). Factors affecting the accuracy of near infrared spectroscopy concentration calculations for focal changes in oxygenation parameters. *Neuroimage*. 18, 865–879.

Suzuki, M., Miyai, I., Ono, T., Oda, I., Konishi, I., Kochiyama, T., Kubota, K. (2004). Prefrontal and premotor cortices are involved in adapting walking and running speed on the treadmill: an optical imaging study. *Neuroimage*. 23, 1020–1026.

Symes, E., Ellis, R., Tucker, M. (2006). Visual object affordances: Object orientation. *Acta psychologica*, *124*(2), 238-255.

Taira, M., Mine, S., Georgopoulos, A. P., Murata, A., and Sakata, H. (1990). Parietal cortex neurons of the monkey related to the visual guidance of hand movement. *Exp. Brain Res*. 83, 29–36.

Tak, S., Ye, JC. (2014). Statistical analysis of fNIRS data: a comprehensive review. *NeuroImage*. 85: 72–91.

Tamura, M., Hoshi, Y., Hazeki, O., & Okada, F. (1997). Cerebral oxygenation states as revealed by near-infrared spectrophotometry. *Advances in Experimental Medicine & Biology*, 413: 91–96.

Tanaka, S., Honda, M., Sadato, N. (2005). Modality-Specific Cognitive Function of Medial and Lateral Human Brodmann Area 6. *The Journal of Neuroscience*. 25(2): 496 –501.

Tanji, J. (1984). The neuronal activity in the supplementary motor area of primates. *Trends Neurosci*. 27: 282-285.

Tanji, J. (1996). New concepts of the supplementary motor area. *Curr Opin Neurobiol*. 6: 782-787.

Tanji, J., Shima, K. (1994). Role for supplementary motor area cells in planning several movements ahead. *Nature*. 371: 413– 416.

Tillas, A., Vosgerau, G., Seuchter, T., Caiani, S. (2017). Can affordances explain behavior? *Review of Philosophy and Psychology*. 8: 295-315.

Toronov, V., Franceschini, M.A., Filiaci, M., Fantini, S., Wolf, M., Michalos, A., Gratton, E. (2000). Near-infrared study of fluctuations in cerebral hemodynamics during rest andmotor stimulation: temporal analysis and spatial mapping. *Med. Phys*. 27, 801–815.

Toronov, V., Webb, A., Choi, J.H., Wolf, M., Michalos, A., Gratton, E., Hueber, D. (2001).Investigation of human brain hemodynamics by simultaneous near infrared spectroscopy and functional magnetic resonance imaging. *Med. Phys*. 28, 521–527.

Tremblay, J., Martínez-Montes, E., Vannasing, P., Nguyen, D., Sawan, M., Lepore, F., Gallagher, A. (2018). Comparison of source localization techniques in diffuse optical tomography for fNIRS application using a realistic head model. *Biomedical Optics*. https://doi.org/10.1364/BOE.9.002994.

Tucker, M., Ellis, R. (1998). On the relations between seen objects and components of potential actions. *Journal of Experimental Psychology: Human Perception and Performance*, 24(3), 830-846.

Ungerleider, L. G., Mishkin, M. (1982). Two cortical visual systems. *Analysis of Visual Behavior*, eds D. J. Ingle, M. A. Goodale, and R. J. W. Mansfield (Cambrige: MIT Press), 549–586.

Vainio, L., Ellis, R., Tucker, M. (2007). The role of visual attention in action priming. *The Quarterly Journal of Experimental Psychology*. 60:2, 241-261.

Van der Zee, P., Delpy, D. (1987). Simulation of the point spread function for light in tissue by a monte carlo method. *Adv Exp Med Biol*. 215: 179–91.

Van Ooteghem, K., Lakhani, B., Akram, S., Miyasike Da Silva, V., McIlroy, WE. (2013). Time to disengage: holding an object influences the execution of rapid compensatory reach-to-grasp reactions for recovery from whole-body instability. *Exp. Brain Res*. 231: 191–199.

Vargas-Irwin, C., Franquemont, L., Black, M., Donoghue, J. (2015). Linking objects to actions: encoding of target object and grasping strategy in primate ventral premotor cortex. *J Neurosci*. 35(30):10888–10897.

Vingerhoets, G., Vandamme, K., Vercammen, A. (2009). Conceptual and physical object qualities contribute differently to motor affordances. *Brain and Cognition*. 69, Pages 481-489.

Villringer, A., Dirnagl, U. (1995). Coupling of brain activity and cerebral blood flow: basis of functional neuroimaging. *Cerebrovasc Brain Metab Rev* 7:240–276.

Villringer, A., Chance, B. (1997). Non-invasive optical spectroscopy and imaging of human brain function. *Trends in Neurosciences*, 20(10), 435–442.

Walker, E., Perreault, E.J. (2015). Arm dominance affects feedforward strategy more than feedback sensitivity during a postural task. *Exp. Brain Res*. 233, 2001 2011.

Watanabe, E., Yamashita, Y., Maki, A., Ito, Y., Koizumi, H. (1996). Non-invasive functional mapping with multi-channel near infra-red spectroscopic topography in humans. *Neurosci. Lett*. 205, 41–44.

Webb, W. (2017). Neurology for the speech-language pathologist (sixth edition). (Elsevier, Missouri).

Weinrich, M., Wise, S. (1982). The premotor cortex of the monkey. *The Journal of Neuroscience*. 2: 1329-1345.

Wise, S. (1985). The primate premotor cortex: past, present, and preparatory. *Annu Rev Neurosci.* 8:1–19.

Wolf, M., Wolf, U., Toronov, V., Michalos, A., Panuescu, L.A., Choi, J.H., Gratton, E. (2002). Different time evolution of oxyhemoglobin and deoxyhemoglobin concentration changes in the visual and motor cortices during functional stimulation: a near- infrared spectroscopy study. *Neuroimag*e 16, 704–712.

Wriessnegger, S., Kurzmann, J., Neuper, C. (2008). Spatio-temporal differences in brain oxygenation between movement execution and imagery: a multichannel near infrared spectroscopy study. *Int J Psychophysiol*. 67(1):54-63.

Yücel, M., Selb, J., Cooper, R., Boas, D. (2014). Targeted principle component analysis: a new motion artifact correction approach for near-infrared spectroscopy. *J Innov Opt Health Sci*. doi:10.1142/S1793545813500661.

Kaiser, V., Gauernfeind, G., Kreilinger, A., Kaufmann, T., Kubler, A., Neuper, C., et al. (2014).Cortical effects of user training in a motor imagery based brain-computer interface measured by fNIRS and EEG. *Neuroimage* 85, 432–444. doi: 10.1016/j.neuroimage.2013.04.097

Zehr, E.P. et al. (2004). Possible contributions of CPG activity to the control of rhythmic human arm movement. *Can. J. Physiol. Pharmacol*. 82, 556–568

Zhang, Y., Brooks, D.H., Franceschini, M.A., Boas, D.A. (2005). Eigenvector-based spatial filtering for reduction of physiological interference in diffuse optical imaging. *J. Biomed.* Opt. 10 (1), 011014.

Zettel, J., Holbeche, A., McIlroy, W., Maki, B. (2005). Redirection of gaze and switching of attention during rapid stepping reactions evoked by unpredictable postural perturbation. *Exp. Brain Res*. 165, 392– 401.

Zettel, J., Scovil, C., McIlroy, W., Maki, B. (2007). Gaze behavior governing balance recovery in an unfamiliar and complex environment. *Neurosci. Lett*. 422, 207 212.